

Observatoire astronomique de Strasbourg  
11 Rue de l'Université  
67000 Strasbourg



Université de Strasbourg  
4 rue Blaise Pascal  
67081 Strasbourg

CROMBEZ, Sébastien  
2019

Master dissertation to obtain the diploma of  
**Master 2 research**  
Mention  
**Astrophysics**  
Jointly accredited by  
**Observatoire astronomique de Strasbourg**  
&  
**Université de Strasbourg**

## SEARCH OF PLANETS, RING AND SATELLITES IN $\beta$ -PICTORIS SYSTEM



Institut de Planétologie  
et d'Astrophysique  
de Grenoble

Institut de Planétologie et  
d'Astrophysique de Grenoble  
414, Rue de la Piscine, Domaine  
Universitaire  
38400 Saint-Martin d'Hères

**Internship supervisor :**

**Dr.Anne-Marie Lagrange**  
Directrice de recherche au CNRS  
Tel : +33 4 76 51 42 03  
**E-mail :**  
[anne-marie.lagrange@univ-grenoble-alpes.fr](mailto:anne-marie.lagrange@univ-grenoble-alpes.fr)

**Date :** 4 mars - 4 juin 2019

*I would like to thanks :*

**François-Xavier Désert**  
*to have accepted to welcome me to IPAG*

**Anne-Marie Lagrange**  
*for all the advices, all the help she gave me and for the time she spent on it.*

**Pascal Rubini**  
*for his advices and the help that brought me to use Dpass.*

**Nadège Meunier**  
*for having helped and exchanged on specific points of the internship.*

*All the people of IPAG who helped me, advised me and informed me.*

## Table of Contents

<b>1 Institut de Planétologie et d'Astrophysique de Grenoble</b>	<b>1</b>
1.1 Localisation . . . . .	1
1.2 A little bit of History . . . . .	1
1.3 Activities . . . . .	1
1.3.1 Major research themes . . . . .	1
1.3.2 Research teams . . . . .	1
1.4 Partnership . . . . .	1
<b>2 Context</b>	<b>2</b>
2.1 Research and study of exoplanets . . . . .	2
2.1.1 History . . . . .	2
2.1.2 Observational methods . . . . .	2
2.2 $\beta$ -Pictroris system . . . . .	3
2.2.1 The star . . . . .	3
2.2.2 Debris discs . . . . .	3
2.2.3 $\beta$ -Pictroris b . . . . .	4
2.3 The $\beta$ -Pictroris 2017 campaign . . . . .	5
2.4 The TESS spacecraft . . . . .	6
2.4.1 Description of the spacecraft mission . . . . .	6
2.4.2 Data acquisition system . . . . .	7
2.5 The ASTEP mission . . . . .	8
2.5.1 Concordia base . . . . .	8
2.5.2 ASTEP research program . . . . .	8
2.5.3 ASTEP-400 . . . . .	9
2.6 Internship research topic . . . . .	10
2.6.1 Purpose of this project . . . . .	10
2.6.2 Impact of the $\delta$ -Scuti pulsations on RV study . . . . .	10
2.7 Description of the approach used during the internship . . . . .	11
<b>3 Gathering and pretreatment of TESS data</b>	<b>12</b>
3.1 Obtain the light curve of the stars . . . . .	12
3.1.1 Selection of the aperture . . . . .	13
3.1.2 Normalisation of the data . . . . .	14
3.1.3 Additional reference stars . . . . .	15
3.1.4 Analysis of disturbance sources . . . . .	17
3.2 Behaviour of the flux of the reference stars . . . . .	19
3.2.1 The pre-process . . . . .	19
<b>4 Comparison between <math>\beta</math>-Pictroris and the reference stars</b>	<b>21</b>
4.1 Transit identification . . . . .	21
4.2 Identification of the momentum dumps . . . . .	21

4.3	Smoothed light curves . . . . .	22
<b>5</b>	<b>Extraction of the <math>\delta</math>-Scuti pulsations</b>	<b>24</b>
5.1	Dpass . . . . .	24
5.1.1	Genetic algorithms . . . . .	24
5.1.2	Operation of Dpass . . . . .	24
5.2	Iterative algorithms . . . . .	26
5.2.1	Period04 . . . . .	26
5.2.2	Fit_tess . . . . .	26
<b>6</b>	<b>Analysis of the pulsation of <math>\beta</math>-Pictoris</b>	<b>27</b>
6.1	Study of pre-processing of the data . . . . .	27
6.2	Comparative study with Dpass . . . . .	27
6.2.1	Improvement of Dpass . . . . .	28
6.2.2	Comparison of fit algorithms with a synthetic series . . . . .	28
6.3	Creation of the data sets used for the fits . . . . .	29
<b>7</b>	<b>Conclusion</b>	<b>31</b>
7.1	Future work . . . . .	31
7.1.1	Clustering study of the fits . . . . .	31
7.1.2	Analysis of ASTEP data . . . . .	31
<b>References</b>		<b>32</b>
<b>Appendix</b>		<b>34</b>

## List of Figures

2.1	Discovery range of the methods used to detect exoplanets . . . . .	2
2.2	STIS/CCD chorographic image of $\beta$ Pic discs (WedgeB2 observations) . . . . .	3
2.3	Schematic of the planetary system of $\beta$ -Pictoris . . . . .	4
2.4	Ground based missions . . . . .	5
2.5	Space missions . . . . .	5
2.6	Region observed by the satellite . . . . .	6
2.7	Combined view of the cameras . . . . .	6
2.8	Imagette of a source obtained by TESS's instruments . . . . .	7
2.9	Location of Concordia Antarctic Base . . . . .	8
2.10	ASTEP FoV around Bpic . . . . .	9
3.11	Shape of the aperture used to compute the flux of Bpic during the four sectors . . . . .	13
3.12	Raw flux of Bpic obtained with SAP (simple aperture photometry) . . . . .	14
3.13	Flux of the calibrations stars form ASTEP filed . . . . .	15
3.14	Flux of the reference stars in addition to ASTEP's ones . . . . .	16
3.15	Flux of the reference stars on the same CDD as Bpic during sectors 5 to 7 . . . . .	16
3.16	Spatial distribution of the near star and the 3 reference stars . . . . .	17
3.17	Example of distribution of quality flag . . . . .	18
3.18	Flux of the three reference stars computed with PDCSAP pipeline . . . . .	19
3.19	The steps to obtain the final light curves . . . . .	20
4.20	Comparison between smoothed curves of Bpic and HD 41214 . . . . .	22
4.21	Comparison between smoothed curves of Bpic and HD 37781 . . . . .	22
4.22	Comparison between smoothed curves of Bpic and HD 40105 . . . . .	23
5.23	Diagram of the operation of dpss . . . . .	25
5.24	Diagram of the operation of period04 . . . . .	26
6.25	Comparison of frequencies obtained in Zieba et al. 2019 and with Dpss . . . . .	27
6.26	Bpic times series of sectors 5 to 7 without the beginning of sector 5 . . . . .	29
6.27	Bpic times series of sectors 5 to 7 without the transits events . . . . .	29
6.28	Bpic times series of sectors 5 to 7 without the transits events and some of end/start time of the orbits . . . . .	30
6.29	Smoothed light curve of Bpic (sectors 5 to 7   sm = 240) . . . . .	30
A.30	Position of $\delta$ Scuti stars in the population I . . . . .	35
B.31	Illustration of the transit methods . . . . .	36
E.32	TESS data, Bpic sectors 5 à 7 . . . . .	39

## List of Tables

2.1	Stellar parameters of $\beta$ -Pictoris	3
2.2	Planetary parameters of $\beta$ -Pictoris b	4
2.3	Planetary parameters of $\beta$ -Pictoris b from Lagrange et al. 2019[21]	4
2.4	Features of TESS instrument	7
3.5	Comparison of the criteria of the two aperture of the lighkurve module	13
3.6	Properties of the selected reference stars	17
3.7	Common flag value during the momentum dumps event	18
4.8	Identification of the momentum dumps (md) in sectors 5 to 7	21
4.9	Reference stars used in Zieba et al. 2019[15]	23
5.10	Type of processes involved in genetic algorithms	24
6.11	Result of the comparative test between Dpass et Tess_fit	28
A.12	Characteristics parameters of the $\delta$ -scuti stars	35
C.13	The status of the members of the Exoplanets team	37
D.14	Sector 4 Observation times	38
D.15	Sector 5 Observation times	38
D.16	Sector 6 Observation times	38
D.17	Sector 7 Observation times	38
E.18	Window definitions	39
F.19	$\delta$ -Scuti frequencies of Bpic found by Zieba et al. 2019	40

## Nomenclature

<i>ASTEP</i>	Antarctica Search for Transiting Extrasolar Planets
<i>Bpic</i>	Abbreviation of $\beta$ -Pictoris
<i>FFI</i>	Full Frame Image
<i>FOV</i>	Field Of View
<i>IPAG</i>	Institut de Planétologie et d’Astrophysique de Grenoble
<i>LC</i>	Light Curves
<i>PDC</i>	Pre-search Data Conditioning
<i>rms</i>	Root Mean Square
<i>RV</i>	Radial Velocity
<i>SAP</i>	Simple Aperture photometry
<i>TESS</i>	Transit Exoplanet Survey Satellite
<i>TF</i>	Transformed Fourier

# 1 Institut de Planétologie et d'Astrophysique de Grenoble

## 1.1 Localisation

The premises of the IPAG<sup>1</sup> are located on the University Park of Saint-Martin-d'Hères in the former premises of the Grenoble Astrophysics Laboratory and in a part of the joint research unit building of the OSUG<sup>2</sup>. This site makes it possible to facilitate the link between the laboratory and the university world. In addition, these premises have allowed brought together the two major centers of research in the sciences of the universe of Grenoble that are planetology and astrophysics.

## 1.2 A little bit of History

IPAG was created in 2011 following the merging of the Grenoble Astrophysics Laboratory and the Grenoble Planetary Laboratory. The laboratory is led by François-Xavier Désert and hosts about 150 people : 60 researchers and teacher-researchers, 30 engineers, technicians and administrative staff, and 60 contracted staff including 20 postdocs and 30 doctoral students or apprentices. IPAG is a joint research unit of the CNRS<sup>3</sup> and Grenoble-Alpes University. It is one of the laboratories of the National Institute of Sciences of the Universe and is part of the Observatory of Sciences of the Universe of Grenoble.

## 1.3 Activities

### 1.3.1 Major research themes

The main research topics of the laboratory are : Stellar and planetary formation, Astrochemistry, Physics of accretion-ejection phenomena around young stellar objects and compact objects, Planetary sciences. Some of the laboratory research teams are involved in instrument developments such as NAOS, WIRCAM, SPHERE, GRAVITY, AMBER, PIONIER...

### 1.3.2 Research teams

- **Planeto:** The study of the small bodies, the planetary atmospheres, surfaces and sub-surfaces of the solar system.
- **Exoplanets:** the detection and characterization of exoplanets. (see Annexe C)
- **Odyssey:** the formation of stars and their planetary procession.
- **Interstellar:** the physico-chemistry of the interstellar medium and the origin of complex molecules.
- **Sherpas:** the processes of accretion-ejection and high-energy emission in young objects and compact objects.
- **Crystal:** the design of the new instruments and detection techniques. The research of technology.

## 1.4 Partnership

The partnership of the laboratory are : UGA, CNRS, CNES<sup>4</sup>, ESO<sup>5</sup> and ANR<sup>6</sup>

<sup>1</sup>Institute of Planetology and Astrophysics of Grenoble, <https://ipag.osug.fr/>

<sup>2</sup>Observatory of Sciences of the Universe of Grenoble <https://www.osug.fr>

<sup>3</sup>National Center for Scientific Research <https://www.cnrs.fr/>

<sup>4</sup>Centre National d'Étude spatiale <https://www.eso.org/public/>

<sup>5</sup>European Southern Observatory <https://www.eso.org/public/>

<sup>6</sup>Agence nationale de recherche, <http://www.agence-nationale-recherche.fr/>

## 2 Context

### 2.1 Research and study of exoplanets

#### 2.1.1 History

The existence of planets gravitating around other stars than the sun was imagined at least since 300 before JC by Epicure ("Nothing opposes the existence of an infinity of worlds" Epicurus in "Letter to Herodotus"). It was not until 1995, with the detection of the planet 51 Pegase b at the Observatoire de Haute-Provence that the existence of extra-solar planets orbiting around a Sun-like star was confirmed. Today, nearly 25 years after the discovery of this first exoplanet, there are more than 4000 exoplanets that have been discovered<sup>7</sup>.

The discovery of these extra-solar planets has led to the emergence of a new area of research, exoplanetology. This field of research is booming with many projects and large scientific experiments such as the new spectroscope SPIROU, EXPRESSO, TESS and soon to be launched KEOPS and JWST. The discovery of exoplanets has allowed the development of new subjects of research within already existing scientific domains such as planetology and astrochemistry.

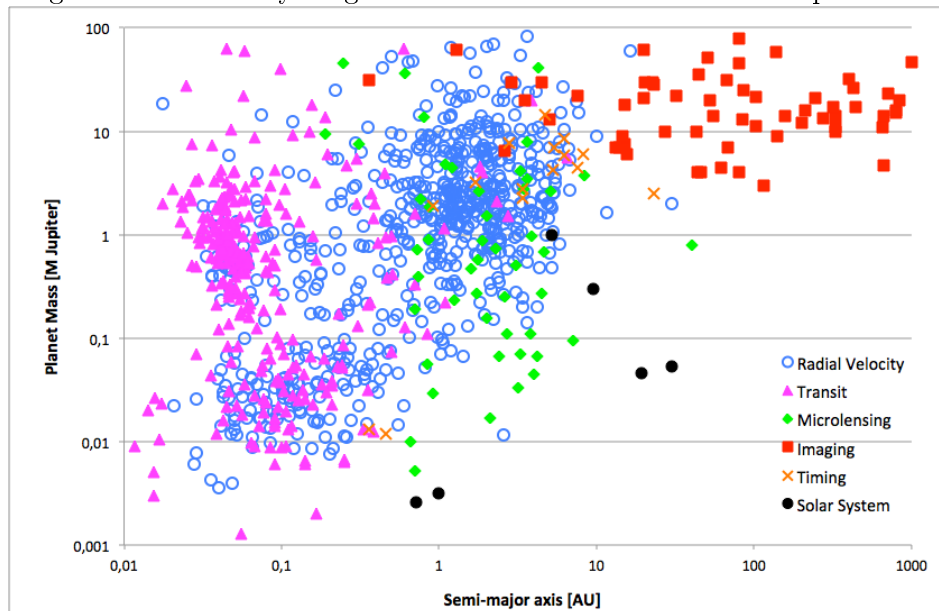
#### 2.1.2 Observational methods

There are 5 main methods to detect exoplanets. Those methods are complementary as they do not provide the same physical parameters of the exoplanets. For instance, transit method give us the radius while the radial velocity gives us the minimum mass. That is why, the research team in which I worked tries to couple the methods available to study the  $\beta$ -Pictoris system. Those methods cover different regions of the exoplanet phase space (fig. 2.1.2). For instance, to study the  $\beta$ -Pictoris system, they first used Direct imaging method to detect the exoplanet  $\beta$ -Pictoris b and now the research team is mainly focus on the Radial Velocity and the Transit method.

Figure 2.1: Discovery range of the methods used to detect exoplanets

#### Detection methods

- Transit (annexe B)
- Radial velocity
- Astrometry
- Direct imaging
- Interferometry*
- Adaptive optics*
- Micro lensing



<sup>7</sup><http://exoplanet.eu/>

## 2.2 $\beta$ -Pictroris system

$\beta$ -Pictroris is the name given to the second brightest star in the constellation of the painter<sup>8</sup>. At the present state of our knowledge the  $\beta$ -Pictroris system is composed of a young star, one debris disk with two components and a giant planet...

### 2.2.1 The star

$\beta$ -Pictroris is a A-type star classified as  $\delta$ -Scuti (see annexe A). Its main parameters of this stars are listed in tab.2.1.

Table 2.1: Stellar parameters of  $\beta$ -Pictroris

Parameter	Value	Source
Total masse ( $M_T$ )	$1.75^{+0.05}_{-0.05} M_{\odot}$	Crifo et al. 1997 [22]
Radius of Bpic ( $R_*$ )	$1.53 R_{\odot}$	Wang et al. 2016 [10]
Age	$23 \pm 3$ Myr	D. Mékarnia et al. 2017 [1]
Spectral type	A5	Simbad
Classe	V	Simbad
magnitude V	3.86	Simbad

### 2.2.2 Debris discs

The star is surrounded by one debris disk which was resolved at optical and near IR wavelengths in the 80-90's, and made of two components[8][18] (see fig.2.2). In 1997 Mouillet and Lagrange proved that the inner wrapped component was due to the presence of a companion object orbiting around the star, later it was found out that the companion was a giant planet  $\beta$ -Pictroris b. The observations obtained with ALMA made it possible to identify a density of CO on the hot disk. This density peaks is about 85 AU from the star[13]. The disc is powered by the evaporation of exocomets and planetesimal collision[4][5][6][7].

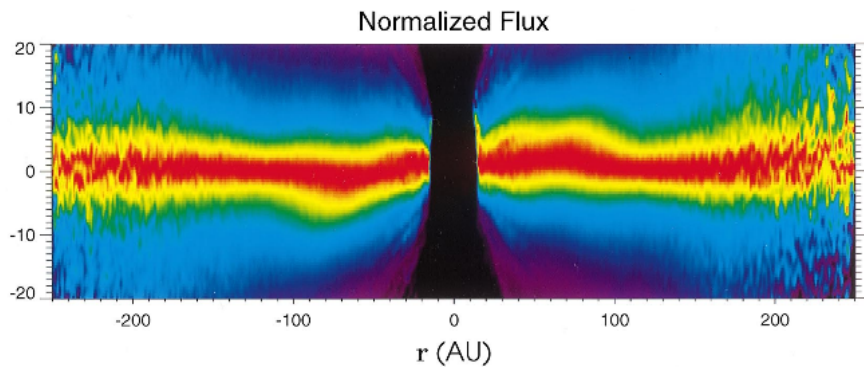


Figure 2.2: STIS/CCD chorographic image of  $\beta$  Pic discs (WedgeB2 observations)  
*Crédit : Heap et al. 2000 [18]*

<sup>8</sup>This constellation is located in the southern part of the celestial sphere, in Latin it is called Pictoris

### 2.2.3 $\beta$ -Pictoris b

This planet was discovered on 18 November 2008 by Anne-Marie Lagrange [3], thanks to the data acquired in 2003 with the NaCo<sup>9</sup> instrument from the VLT<sup>10</sup>.  $\beta$ -Pictoris b is considered to be a giant planet as its mass is about 9 to 12 Jupiter masses. Its physical and orbit parameters are detailed in tab.2.2 and tab.2.3. The value found in Wang et al. 2016[10] based on GPI<sup>11</sup> are a bit different than the one find in Lagrange et al. 2019[21] which are based on SPHERE<sup>12</sup>.

Table 2.2: Planetary parameters of  $\beta$ -Pictoris b

Parameter	Value	Source
Distance (d)	19.3pc	van Leeuwen 2007 [11]
Radius Bpic b ( $R_p$ )	$1.46 \pm 0.01 R_j$	Chilcote et al. 2017 [12]
Inclination Bpic b ( $i$ )	$88.81^\circ \pm 0.12^\circ$	Wang et al. 2016 [10]
Semi major axis ( $a$ )	$9.66^{+1.12}_{-0.64} UA$	Wang et al. 2016 [10]

Crédit : M. Mol Lous et al. 2018 [9]

Table 2.3: Planetary parameters of  $\beta$ -Pictoris b from Lagrange et al. 2019[21]

Parameter	Value
Semi major axis ( $a$ )	$8.90^{+0.25}_{-0.41} UA$
Orbital period (P)	$20.29^{+0.86}_{-1.35}$ yr
Eccentricity (e)	$0.01^{+0.029}_{-0.01}$
Inclination ( $i$ )	$89, 08^{+0.16}_{-0.19}$

Due to the angle under which the Bpic system is observed, Bpic b cannot be detected by the transit method (see appendix B). However, the sphere of Hill<sup>13</sup> of Bpic b should transit in front of Bpic from our point of view. We can therefore hope to observe potential rings or satellites of Bpic b (see Fig.2.3). The last transit of the Hill sphere might have started on April in 2017 and finished at the end of January in 2018 according Wang et al. 2016[10]). According to Lagrange et al. 2019[21] the last transit might have lasted about few weeks around 2017.72 and the next transit might be in 2038.06.

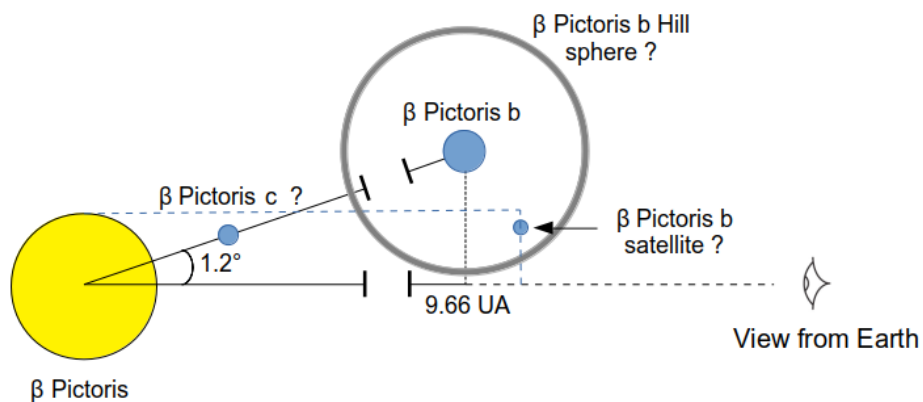


Figure 2.3: Schematic of the planetary system of  $\beta$ -Pictoris

Adapted from de M. Mol Lous et al. 2018 [9]

<sup>9</sup>Adaptive Optics System, see <http://www.eso.org/sci/facilities/paranal/instruments/naco.html>

<sup>10</sup>Very Large Telescope, see [https://en.wikipedia.org/wiki/Very\\_Large\\_Telescope](https://en.wikipedia.org/wiki/Very_Large_Telescope)

<sup>11</sup>Gemini Planet Imager, <https://www.gemini.edu/sciops/instruments/gpi/>

<sup>12</sup>Spectro-Polarimetric High-contrast Exoplanet REsearch <https://www.eso.org/sci/facilities/paranal/instruments/sphere.html>

<sup>13</sup>The sphere of Hill of an astronomical object is the space domain in which it dominates in the phenomenon of attraction of the satellites. The surface of this sphere is a region where the velocity field is zero. To be retained by a planet, a satellite must be in this sphere. see [https://en.wikipedia.org/wiki/Hill\\_sphere](https://en.wikipedia.org/wiki/Hill_sphere)

### 2.3 The $\beta$ -Pictoris 2017 campaign

In 2017, an International team set up an ambitious ground and space based photometric campaign to try to detect and characterize a transit of Bpic b Hill sphere. The campaign was completed by high resolution spectroscopic observations. Part of the missions that study Bpic are ground based (see fig.2.4) and the others based on spacecraft (see fig.2.5).

Figure 2.4: Ground based missions

- **ASTEP<sup>a</sup>**: French mission, which uses a 400m telescope (4kx4k,0.93"/pix,1° FOV) based in Antarctica (Dom C). [Photometry](#)
- **bRing<sup>b</sup>**: Dutch mission based on two 2-camera robotic observatory (5-camera MASCARA system), one based in Australia and the other in South Africa. [Photometry](#)
- **AST3<sup>c</sup>**: Chinese mission, which uses a 680 mm telescope (5kx10k,1"/pix,4° FOV) based in Antarctica (Dom A). [Photometry](#)
- **SALT-HRS<sup>d</sup>** [Spectroscopy](#)
- **HARPS<sup>e</sup>** [Spectroscopy](#)

<sup>a</sup>The Antarctica Search for Transiting Extrasolar Planets

<sup>b</sup>beta pictoris b Ring, <https://www.aanda.org/articles/aa/pdf/2017/11/aa31679-17.pdf>

<sup>c</sup>Antarctic Survey Telescope, (Xiangyan Yuan et al. 2014)

<sup>d</sup>Southern African Large Telescope High Resolution Spectrograph, <https://www.salt.ac.za/telescope/>

<sup>e</sup>High Accuracy Radial velocity Planets Search , <http://www.eso.org/sci/facilities/lasilla/instruments/harps.html>

Figure 2.5: Space missions

- **TESS<sup>a</sup>** Spacecraft dedicated to detect exo-planet transit(operated by NASA and MIT). [Photometry](#)
- **HST<sup>b</sup>** Hubble Space Telescope ( run by NASA,ESA,STScI). [Photometry & Spectroscopy](#)
- **BRITE<sup>c</sup>** Five nanosatellites operated by a consortium of universities from Canada, Austria and Poland. [Photometry](#)
- **PICSAT<sup>d</sup>** French nanostallite aim at monitoring Bpic. [Photometry](#)

<sup>a</sup>Transiting Exoplanet Survey Satellite, see <https://heasarc.gsfc.nasa.gov/docs/tess/>

<sup>b</sup>Hubble Space Telescope, <http://hubblesite.org/>

<sup>c</sup>Bright Target Explorer, <https://brite-constellation.at/>

<sup>d</sup>Beta pictoris nanosatellite, <https://picsat.obspm.fr>

We have decided to use ASTEP Data as they were the best photometric Data available to study the Hill sphere transit of Bpic b. Also we have decided to use TESS Data recording in late 2018 as those data have the best quality to do the measurement of the  $\delta$ -Scuti pulsations of Bpic.

## 2.4 The TESS spacecraft

### 2.4.1 Description of the spacecraft mission

TESS is a satellite developed by NASA. His main mission his to detect exoplanets with the Transit method. He was launched on the 18th of April 2018. It has to monitor about 200 00 dwarfs on the main sequence. To do so, it used four large field camera. It proceeds by measuring sector by sector. The sky is split into 26 sectors, and each sector is split into four squares that correspond the total FOV of the 4 cameras (see fig.2.6).

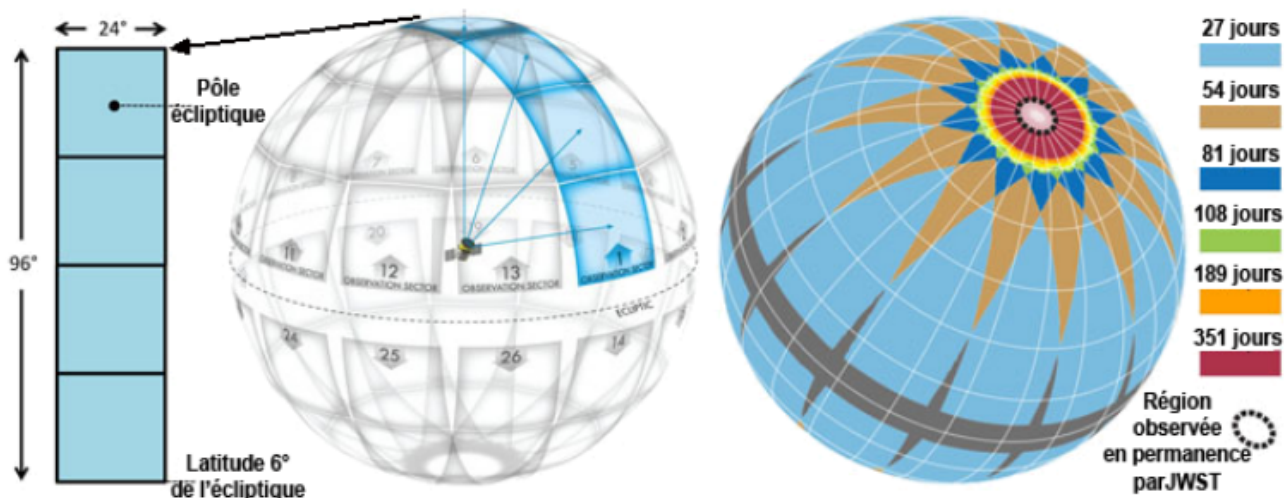


Figure 2.6: Region observed by the satellite

source : [https://tess.gsfc.nasa.gov/images/tess\\_science\\_image3.jpg](https://tess.gsfc.nasa.gov/images/tess_science_image3.jpg)

The flux of the 200 00 preselected targets is recorded every 2 minutes with a resolution of 21 arc seconds / pixel. TESS also obtains full-frame images (FFI) of the entire four-camera field of view (24 x 96 degrees) at a rate of 30 minutes. We can see on fig.2.6 how is distributed the observation time of TESS on a projection of the celestial sphere. We can also see on fig.2.7 an example of full-screen images. For the preselected targets we obtain scientific images like the one shown on fig.2.8.

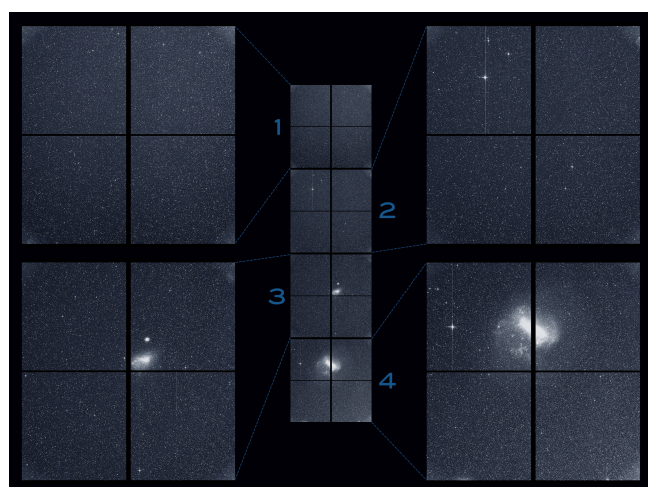


Figure 2.7: Combined view of the cameras

source : <https://heasarc.gsfc.nasa.gov/docs/tess/objectives.html>

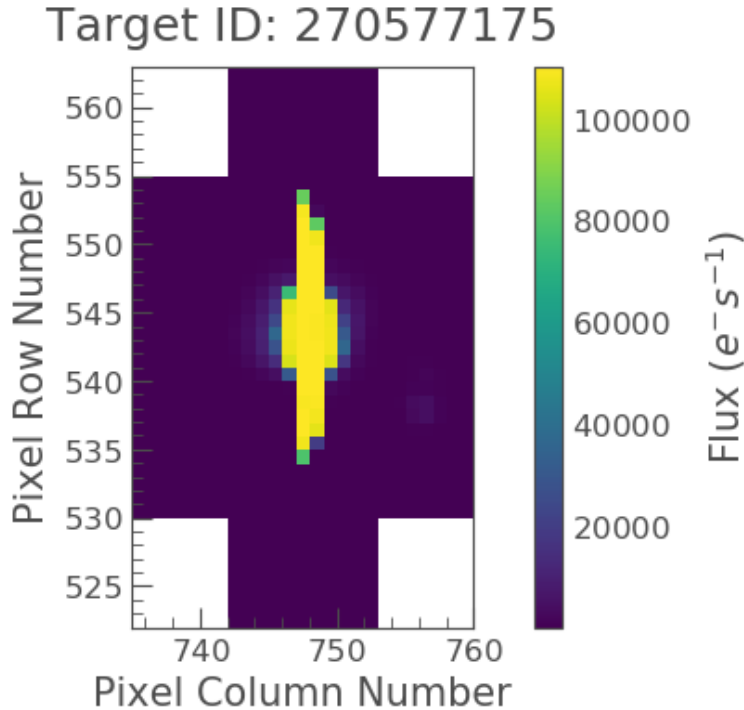


Figure 2.8: Imagette of a source obtained by TESS's instruments

#### 2.4.2 Data acquisition system

The satellite produces mainly two types of data :

- The time series of imagettes (cf fig.2.8) on the predefined targets.
- Scientific image at 30 min rate (cf fig.2.7).

The main feature of the photometric data acquisition system the one shown in tab.2.4:

Characteristic	Value
Number of cameras	4
Field of view	$24^\circ \times 24^\circ$
CCDs	MIT/LL CCID-80
CCDS pear camera	4
CCD dimensions	$2028 \times 2048$ pixels by imaging matrix
Pixel size	$15 \mu\text{m}^2$
Pixel Depth	$100 \mu\text{m}$
Lenses	Lens (146 mm, lens f / 1.4)
Bandwidth	600-1040 nm
Camera temperature	$-85^\circ\text{C}$ (lenses), $-80^\circ\text{C}$ (CCDs)
Portion of sky covered by a pixel	21x21 arc-second $^2$

Table 2.4: Features of TESS instrument  
source : Roland Vanderspek et al. 2018 [14]

## 2.5 The ASTEP mission

### 2.5.1 Concordia base

Concordia is a French-Italian research station based on the Antarctic plateau<sup>14</sup> (see fig.2.9). It was created in 1995 in order to have a second base more inland. This base can accommodate sixty people during the summer, but during the wintering periods the maximal number drops to fifteen people. With polar nights for three months, an exceptional sky quality due to its location at an altitude of 3,233 m and clear sky 80 % of the time, this site allows long astronomical observations over this period.

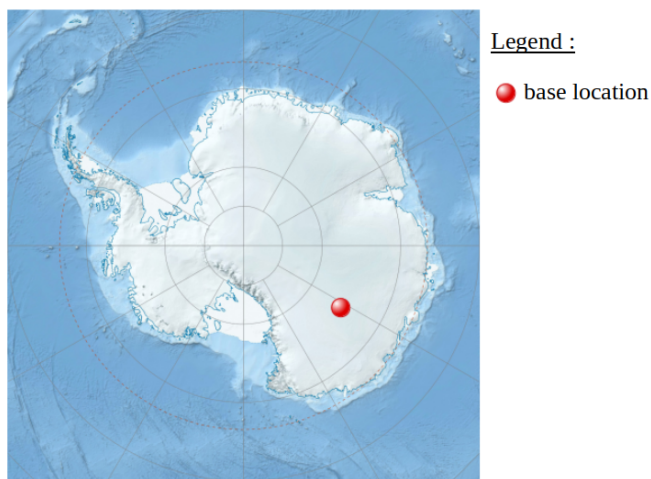


Figure 2.9: Location of Concordia Antarctic Base

source : [https://commons.wikimedia.org/wiki/File:Antarctica\\_relief\\_location\\_map.jpg](https://commons.wikimedia.org/wiki/File:Antarctica_relief_location_map.jpg)

### 2.5.2 ASTEP research program

ASTEP was installed in 2009. This project is mainly supported by IPEV<sup>15</sup>. This scientific program is composed of two instruments :

- **ASTEP-south** A 10 cm fixed telescope, which continually points to the celestial south pole.
- **ASTEP-400** A 400 mm automated telescope, which observed  $\beta$ -Pictoris for the purpose of detecting variations related to the transit of the Hill sphere of the planet in 2017-2018  $\beta$ -Pictoris b.

<sup>14</sup>[https://fr.wikipedia.org/wiki/Base\\_antarctique\\_Concordia](https://fr.wikipedia.org/wiki/Base_antarctique_Concordia)

<sup>15</sup>Institut polaire français Paul-Émile Victor, <https://www.institut-polaire.fr/language/fr/>

### 2.5.3 ASTEP-400

The scientific image obtained with ASTEP-400 are defocused (see fig.2.10). This is because the star  $\beta$ -Pictoris is very bright ( $V = 3.85$ ).



Figure 2.10: ASTEP FoV around Bpic

## 2.6 Internship research topic

### 2.6.1 Purpose of this project

The main purpose of my internship was initially to analyse the photometric data of  $\beta$ -Pictoris that were acquired during the winter measurement campaign of 2017-2018 as part of the ASTEP mission (see § 2.5), in order to detect potential signatures of the transit of the planet Hill sphere  $\beta$ -Pictoris b.

To detect such transit it is necessary to clean up the signal of all parasitic noises as well as the stellar pulsations that result from Bpic's stellar activity. In D. Mekarnia et al. 2017 [1] they showed that indeed the pulsations dominate the photometric variability.

The ASTEP data have been acquired on the ground, so that they are quite noisy due to the atmosphere, the moon light and the sun light. Also, sometimes an ice film formed on the instrument. It turns out that it was harder than expected to correct the effect on data due to this ice film.

We realized soon that using the recently released high quality photometric TESS data (see § 2.4) would allow us to extract the pulsation patterns in an excellent way, as the data are of excellent quality. It was then decided to start working on the TESS data, and use the results obtained to possibly analyse, in a second step, the ASTEP data.

### 2.6.2 Impact of the $\delta$ -Scuti pulsations on RV study

$\beta$ -Pictoris pulsations significantly impact the radial velocity variations. A better identification of the pulsations of Bpic would help to correct the effects of those the pulsations on the radial velocity measurements in order to obtain more accurate results and detect Bpic or other planets signal(s). So the pulsations identified in photometry would be used in a later stage for the spectroscopic analysis.

## 2.7 Description of the approach used during the internship

We have decided to split the internship in two parts.

First, study the data from **TESS** to analyse the pulsations of  $\beta$ -Pictoris and then study the transit with **ASTEP** data.

The analysis of TESS data was decomposed in three parts :

- The extraction of and the preprocessing of the light curve.
- The comparative study with reference stars.
- The analysis of the  $\delta$ -Scuti pulsations with **Dpass**.

Finally, most of the internship was spent on the TESS data. This is because :

- First the careful data extraction was made took much longer than expected. We succeeded in extracting optimally the data, and analysing the pulsation pattern of Bpic.
- Second, shortly after the beginning of the internship, another team submitted a paper describing the discovery of comets transit in the same TESS data. We decided then to see if we could confirm their discovery using our own extraction analysing tools. It turned out that the tools we developed are more efficient than the classical ones they used.

The analysis of the ASTEP data that was planned to be in two parts.

- First, the extraction of the  $\delta$ -Scuti pulsations in ASTEP data and the comparison of those pulsations with the one found with TESS data.
- Then the analysis of the residue of the ASTEP data fit, in order to see if we detect the signature of the transit of the Hill sphere of  $\beta$ -Pictoris b.

### 3 Gathering and pretreatment of TESS data

#### 3.1 Obtain the light curve of the stars

The first task assigned to me was to study the availability of photometric data obtained with the TESS satellite (see § 2.4) of Bpic and the reference stars that are present in the ASTEP FoV (see fig.2.10). I went through the **MAST**<sup>16</sup> to identify the reference stars that have high speed photometric data available in this archive. Then, I wrote a python script to retrieve the photometric data thanks to the module **lightkurve**<sup>17</sup>. To extract the light curves, it is necessary to compute the photometric flux of the star on each image (see Fig.2.8). However, there are two basic possibilities, the first is to integrate on all the imagettes (opening = "all") and the second to use an optimum mask that is provided with the data to integrate only on the pixels of interest (opening = `data.pipeline_mask`) see example fig.3.11.

In order to find out the best aperture to extract the light curves, I have computed the difference between the outputs of the two methods and the division.

Let  $d_1 = \{d_{1,1}, d_{1,2}, \dots, d_{1,N}\}_{N \in \mathbb{N}}$  and  $d_2 = \{d_{2,1}, d_{2,2}, \dots, d_{2,N}\}_{N \in \mathbb{N}}$  the photometric data obtained from the same imagette but using two different masks to integrate the stream.

Computation of the difference with the standard L1 (`diff_mask_L1`):

$$\|d_1 - d_2\|_1 = \frac{1}{N} \sum_{i=1}^N |d_{1,i} - d_{2,i}| \quad (3.1)$$

Computation of the difference with the norm L2 (`diff_mask_L2`):

$$\|d_1 - d_2\|_2 = \sqrt{\frac{1}{N} \left[ \sum_{i=1}^N (d_{1,i} - d_{2,i})^2 \right]} \quad (3.2)$$

Computation of the ratio (div):

$$\left\| \frac{d_1}{d_2} \right\|_1 = \frac{1}{N} \sum_{i=1}^N \left| \frac{d_{1,i}}{d_{2,i}} \right| \quad (3.3)$$

The computation of the distance between the data obtained with the opening "all" and the data obtained the intrinsic opening provided in the pipelines of the module **lightkurve** (`data.pipeline_mask`) for the photometric data of Bpic reveals the existence of an almost constant offset between the two datasets. This difference is due to the fact that when one uses the opening "all" to compute the flux, one takes into account in all the cases the flux of the star but also, the rest of the flux form background of the imagettes. Surprisingly this background flux is not null (see fig. 3.11).

<sup>16</sup>Mikulski Archive for Space Telescopes portal, see <https://archive.stsci.edu/>

<sup>17</sup>Python module specially developed to process the KEPLER and TESS satellites data

### 3.1.1 Selection of the aperture

Aperture	Pro	Cons
"all"	Always compute at least the flux of the star	Highly sensitive to variations of the flux
intrinsic	Optimised to only compute the flux of the star	Use of a black box

Table 3.5: Comparison of the criteria of the two aperture of the lighkurve module

We have studied the Pro and cons of the two filters (see table 3.5) and we decided to use the filter provided by the pipeline. However, Later on following a closer study of the Handbook of TESS [14] allowed to raise in part the black box side of filter and allowed us to strengthen our choice. Also we could have define ourselves the form of the aperture.

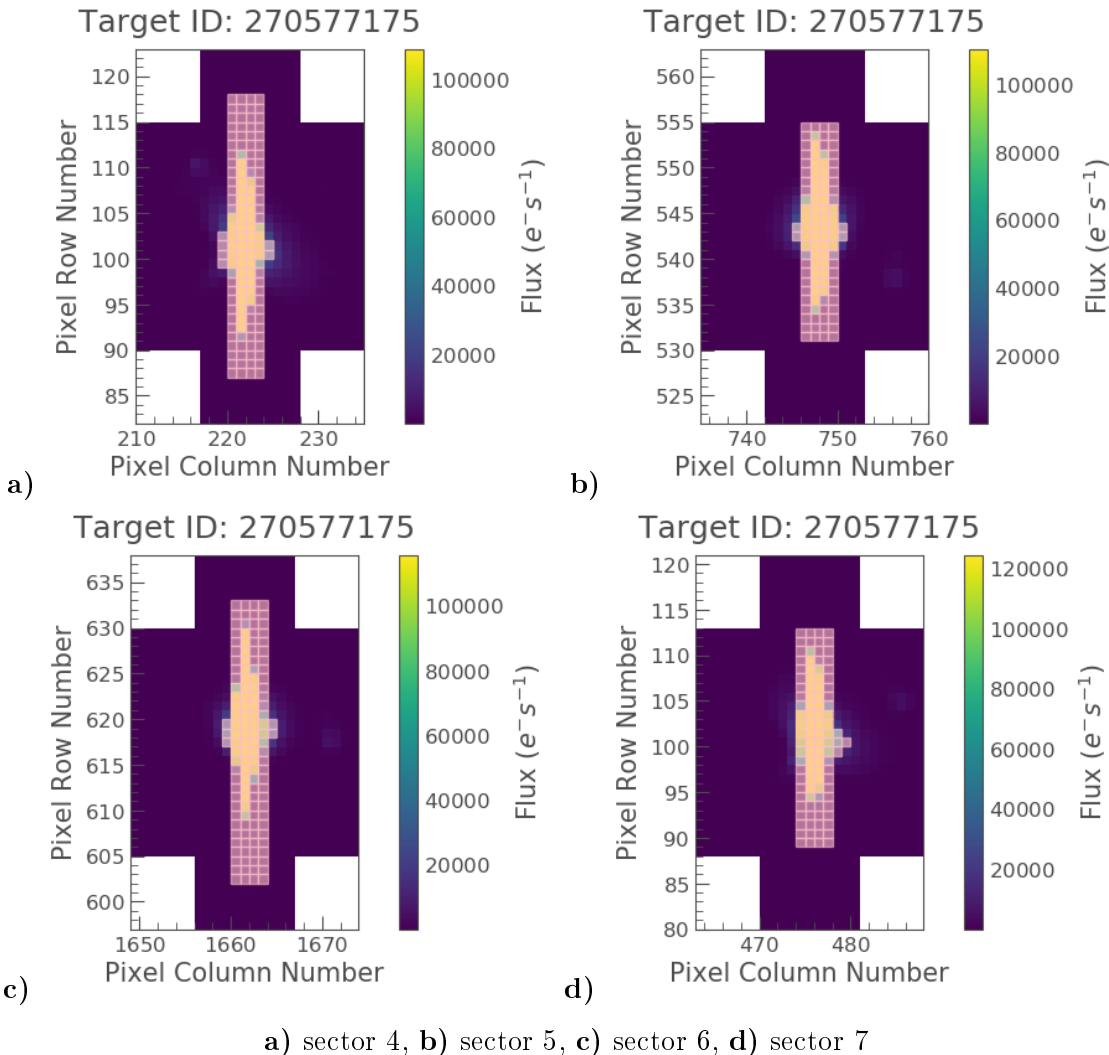


Figure 3.11: Shape of the aperture used to compute the flux of Bpic during the four sectors

The aperture varies a bit from one sector to another ( see fig.3.11. This shape is due to effects such as blooming, which is due to the conception of TESS CDD (§ 6.7.1 [14]).

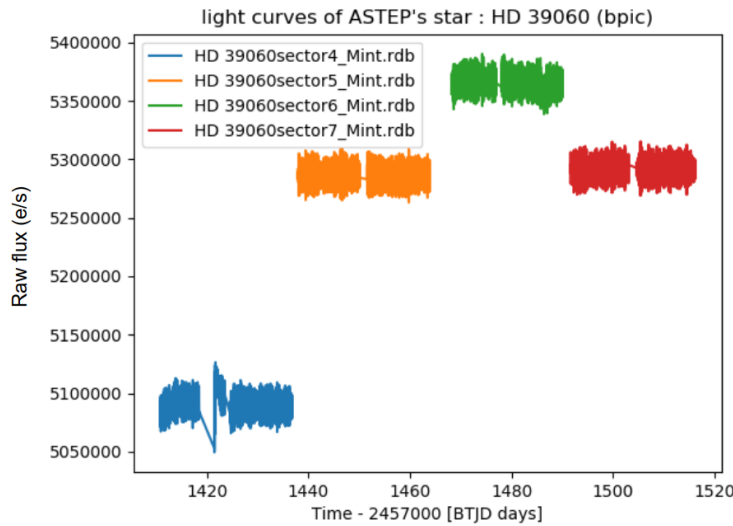


Figure 3.12: Raw flux of Bpic obtained with SAP (simple aperture photometry)

Now that we obtained the flux of Bpic and the reference star (see example of raw flux fig.3.12), we have to normalize the flux of the star.

We noticed that the data obtained in sector 4 for Bpic and the reference stars were of particularly bad quality (see fig.3.12). This was due to an issue with the guiding stars around 1413.26 BTJD (cf tab.D.14).

### 3.1.2 Normalisation of the data

Then, we have to normalise the data. To do so we apply the normalisation with the median (eq.3.4) to the photometric fluxes. I have used the function **median** from the module **statistics**<sup>18</sup> de **python** to obtain the median in order to normalise sector by sector.

$$F(t)_{normalize} = \frac{F(t)}{F_{median}} \quad (3.4)$$

We also have to clean the data. To do so I have used the functions of the class **TessLightCurve**<sup>19</sup> of the module **lightkurve** :

- `remove_nans()`
- `remove_outliers()`

In order to quantify the effect of those functions and to have a tool which allows us to compare the modifications that we have done to the data. We used the root mean square of the data (eq.3.5).The study of the rms variations between the data before and after using the `remove_nans()` and `remove_outliers()` functions for each sector revealed that the functions `remove_nans()` has no effect on the last 3 sectors. These functions only had effect on the sector 4, due to the spacecraft guiding issues that happened during this sector(see cf tab.D.14).

$$rms_{d_1} = \sqrt{\frac{1}{N} \sum_{i=1}^N d_1(i)} \quad (3.5)$$

<sup>18</sup><https://docs.python.org/3/library/statistics.html>

<sup>19</sup><http://docs.lightkurve.org/api/lightkurve.lightcurve.TessLightCurve.html>

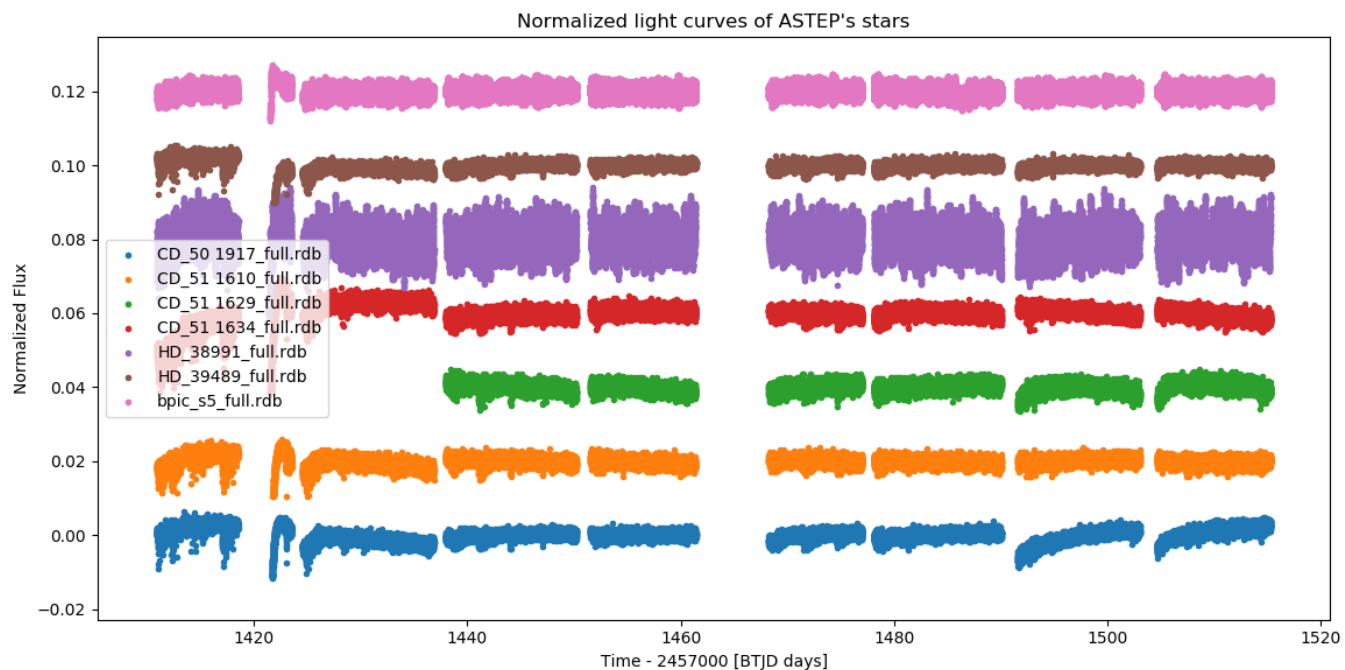


Figure 3.13: Flux of the calibrations stars form ASTEP file

After applying the normalisation and plotting together the flux of the ASTEP stars, we observed that HD 38991 is a variable star and the flux of the other stars seem to be distorted but not in the same way (see fig.3.13).

### 3.1.3 Additional reference stars

In order to be able to better understand the behaviour the photometric data obtained by the TESS satellite. I looked for reference stars in addition to the ones within the ASTEP FoV (see Fig.2.10). I have tried to find stars that were not too far from Bpic and brighter in the field of view of ASTEP. To do this I used **Aladin**<sup>20</sup> and coupled with **Simbad**<sup>21</sup>. The goal was to find stars with a lower magnitude than the ones already listed in the ASTEP field, in order to have photometric data less sensitive to noise. Then I checked that those stars had data type "time series" available through the portal **MAST**. In order to then recover the photometric data with the module **lightkurve**.

When we plot together the flux of the reference stars (see fig.3.13 and fig.3.14), we do observe that, the flux of the stars is degraded in quite a different way even if some of them seems to have been degraded the same way on some sectors. It appears that most of the calibrations were not on the same CCD of the same camera on each sector. I had found the document where were stored the name of the targets plus the number of the CCD and the camera that have acquired their flux during a sector. Thanks to this document have been able to identified which stars were on the same CCD as Bpic during the sectors 5 to 7.

We decided to keep the start that fulfilled the following conditions :  $TESS_{mag} < 7$  **AND** Star on the same CDD as Bpic during sectors 5 to 7 **AND** as close as possible to Bpic  
We final keep the three brightest stars (HD 41214, HD 37781, HD 40105 see fig.3.15) whose main parameters are defined in tab.3.6.

<sup>20</sup>Professional Atlas of the sky, see <https://aladin.u-strasbg.fr/>

<sup>21</sup>Astrophysical Database, see <http://simbad.u-strasbg.fr/simbad/>

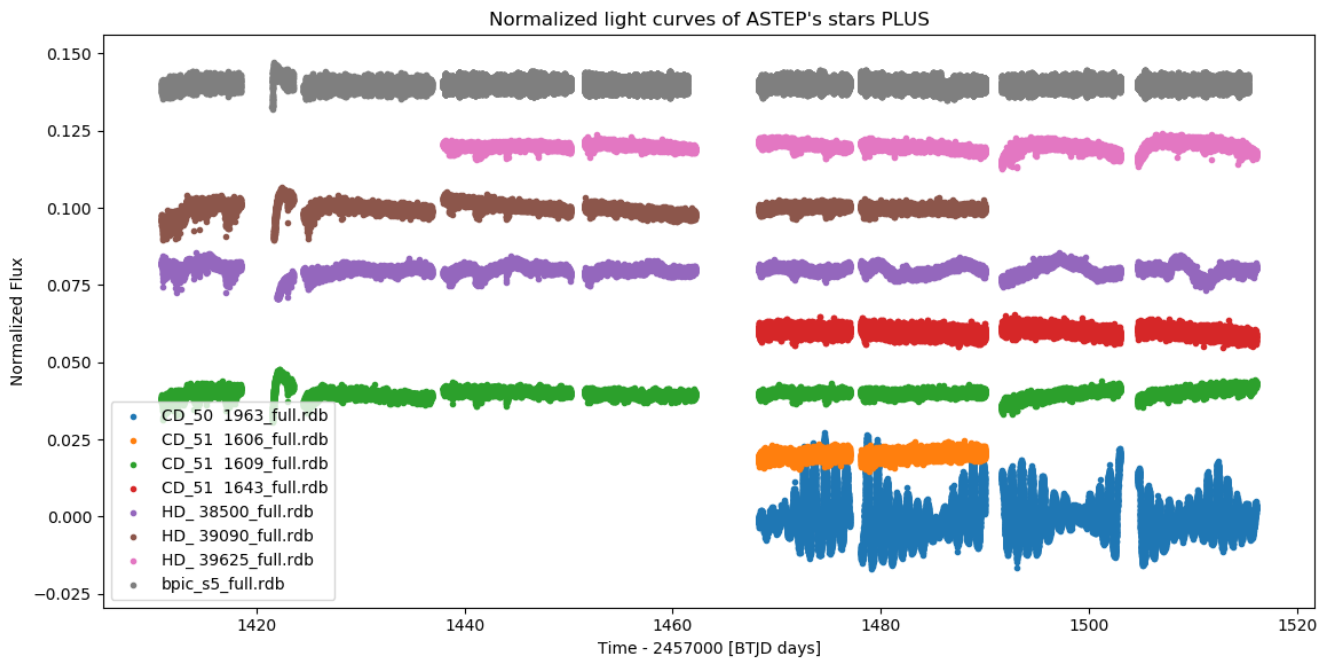


Figure 3.14: Flux of the reference stars in addition to ASTEP's ones

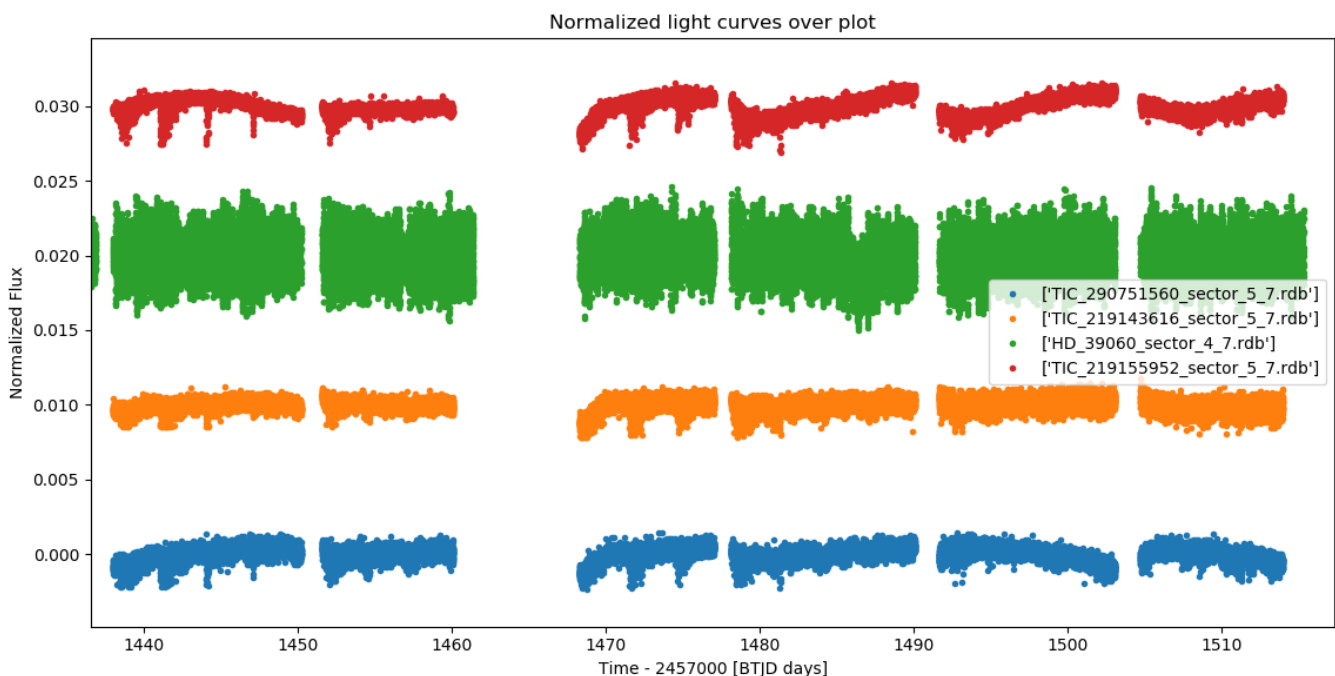


Figure 3.15: Flux of the reference stars on the same CDD as Bpic during sectors 5 to 7

As the three stars still show different types of low frequencies variations. We observed especially in the time interval 1439-1450 BTJD and 1468-1477 BTJD, a repetitive pattern which might result of the momentum dumps (see § 3.1.4). So I had to find a way to remove the data that were distorted during the momentum dumps and understand why even if i try to select non-variable that have been measured on the same CCD as Bpic show various types of alterations.

I decided to watch other stars who were closest to Bpic ( see fig.3.16) to see if they have the same alteration in there flux(see fig.3.16). Its appears that, also the star quite near to Bpic still don't show the same alteration in there flux.

	<b>HD 41214</b>	<b>HD 37781</b>	<b>HD 40105</b>
TESS identifier	TIC 219155952	TIC 290751560	TIC 219143616
V mag	5.647	6.42	6.52
RA	06 00 49.1704836808	05 38 17.4206791230	05 54 10.8134085143
DEC	-51 12 58.767549937	-50 38 27.584072051	-50 21 45.181145969
Sp type	A1mA3-A7	A0V	K1IV-V
Distance to Bpic	2, 13° ± 0, 01°	1, 48° ± 0, 01°	1, 29° ± 0, 01°

Table 3.6: Properties of the selected reference stars



blue : Bpic / red : HD 41214 / green : HD 37781 / yellow : HD 40105 / purple : the nears stars

Figure 3.16: Spatial distribution of the near star and the 3 reference stars

### 3.1.4 Analysis of disturbance sources

The data collected by the spacecraft are subject to various sources of disturbance. Most of those perturbations (read out noise, bias, saturation, cosmic ray...) are automatically treated by the pipeline that calibrated the imagettes used to compute the light (cf § 6 [14]).

One of the main source of disturbance in the flux of the stars is due to the momentum dumps that happened every 2-3 days due to the necessity to use thruster firings to maintain positioning of the spacecraft. Because of that, the pointing jitter decrease during the manoeuvre.

For each sector produced by **TESS** a Data Release note paper is created. In order to give an overview of the events that appended during the acquisition and the statistical data about the potential transit detected by automatic detection processes [16].

- TESS Data Release Notes : Sector 4, DR5 [https://archive.stsci.edu/missions/tess/doc/tess\\_drn/tess\\_sector\\_04\\_drn05\\_v04.pdf](https://archive.stsci.edu/missions/tess/doc/tess_drn/tess_sector_04_drn05_v04.pdf)
- TESS Data Release Notes : Sector 5, DR7 [https://archive.stsci.edu/missions/tess/doc/tess\\_drn/tess\\_sector\\_05\\_drn07\\_v02.pdf](https://archive.stsci.edu/missions/tess/doc/tess_drn/tess_sector_05_drn07_v02.pdf)
- TESS Data Release Notes : Sector 6, DR8 [https://archive.stsci.edu/missions/tess/doc/tess\\_drn/tess\\_sector\\_06\\_drn08\\_v02.pdf](https://archive.stsci.edu/missions/tess/doc/tess_drn/tess_sector_06_drn08_v02.pdf)
- TESS Data Release Notes : Sector 7, DR9 [https://archive.stsci.edu/missions/tess/doc/tess\\_drn/tess\\_sector\\_07\\_drn09\\_v03.pdf](https://archive.stsci.edu/missions/tess/doc/tess_drn/tess_sector_07_drn09_v03.pdf)

The quality of all data acquired by TESS is evaluated and stored in "QUALITY" field. This field contains an integer, a zero value its mean that no errors were detected. Otherwise, if some errors were detected the value will be a power of two and the decomposition in elementary power of two will give the value of the errors that appended during the acquisition of the sector (see 3.17). The description of the flag can be found in § 9 [20].

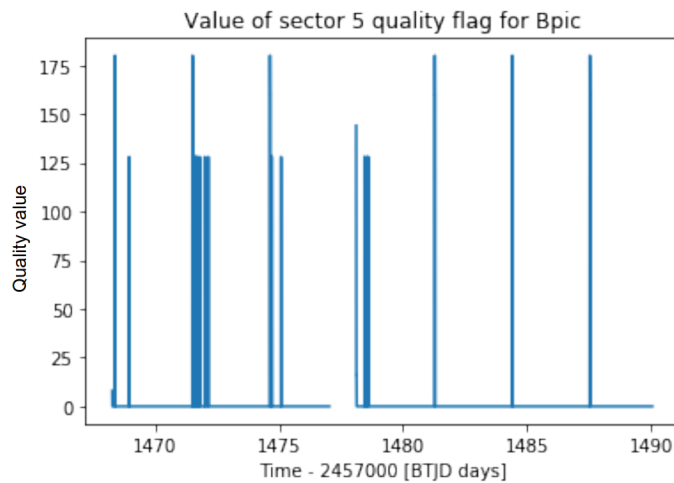


Figure 3.17: Example of distribution of quality flag

Thanks to this flag we could identify the momentum dumps. At first glance, it is possible to identify repetitive peaks in the quality data (see fig.3.17). If we decompose the Quality values, we might be able to identify clearly the location of the momentum dumps as they correspond to a flag value of 32. After analysis, the quality flag to find that the period of appearance of the momentum dumps corresponds to the one given in the Data Release note documents. The momentum dumps last about 4 to 18 minutes which is in agreement with the § 8.2.4 [14]. Most of the time, during the momentum dumps we found the groups of errors flag show in tab.3.7.

Value of the Quality	Corresponding flags
176	Manual Exclude (128) Reaction Wheel desaturation Event (32) Argabrightening event (16)
180	Manual Exclude (128) Reaction Wheel desaturation Event (32) Argabrightening event (16) Spacecraft is in Coarse Point (4)
160	Manual Exclude (128) Reaction Wheel desaturation Event (32)

Table 3.7: Common flag value during the momentum dumps event

### 3.2 Behaviour of the flux of the reference stars

At first we have used the SAP (simple aperture photometry). Which consists in calculating the flux of the star imagette by imagette by integrating the flux inside the aperture. After that, we removed the outlier and the *nan* values. As these pre-treatments do not make it possible to obtain curves which allow a good comparison between reference stars and Bpic.

So that have investigated how to manage this point, and I have found out that the PDCSAP [19] pipeline can help to obtain flux more relevant to do the comparison between Bpic and the referenced stars. As the main goals of the PDC (Pre-search Data Conditioning) is to manage the systematic errors due to the instrument. These instrumental errors are one of the main reason why the flux of the referenced stars appear to be quite different.

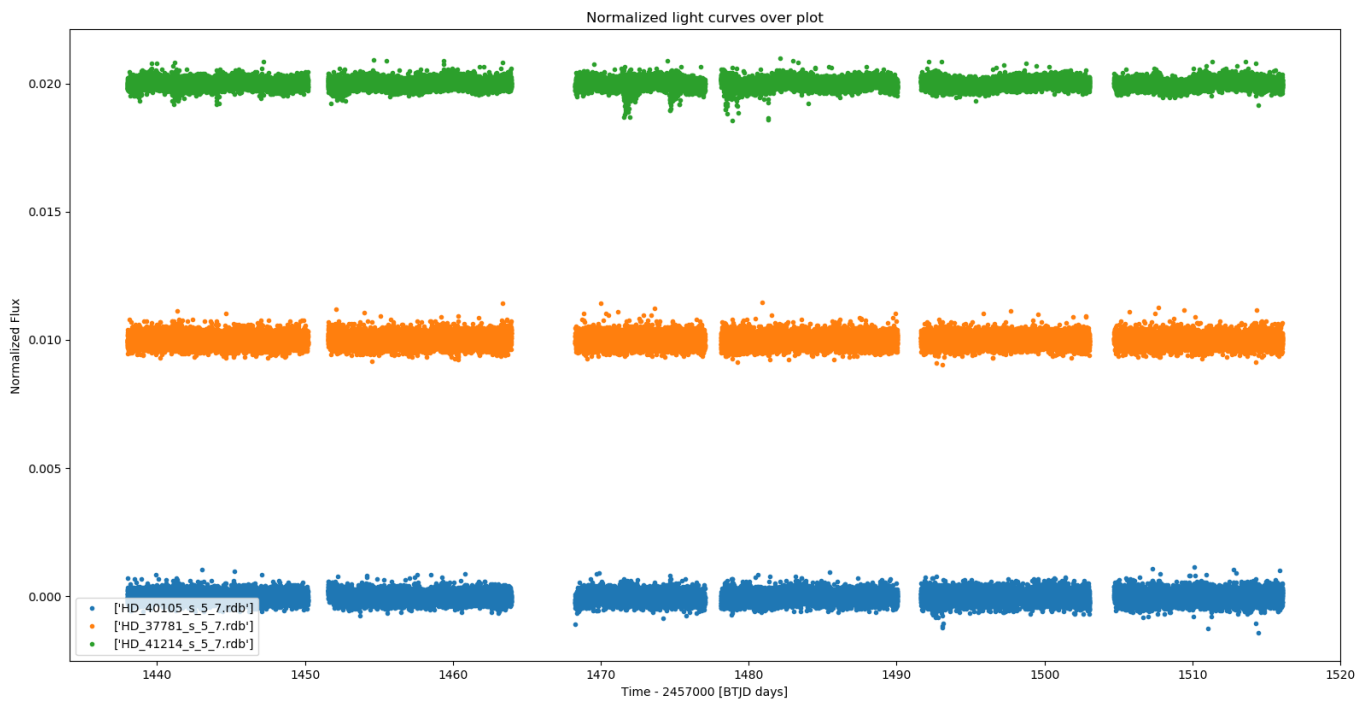
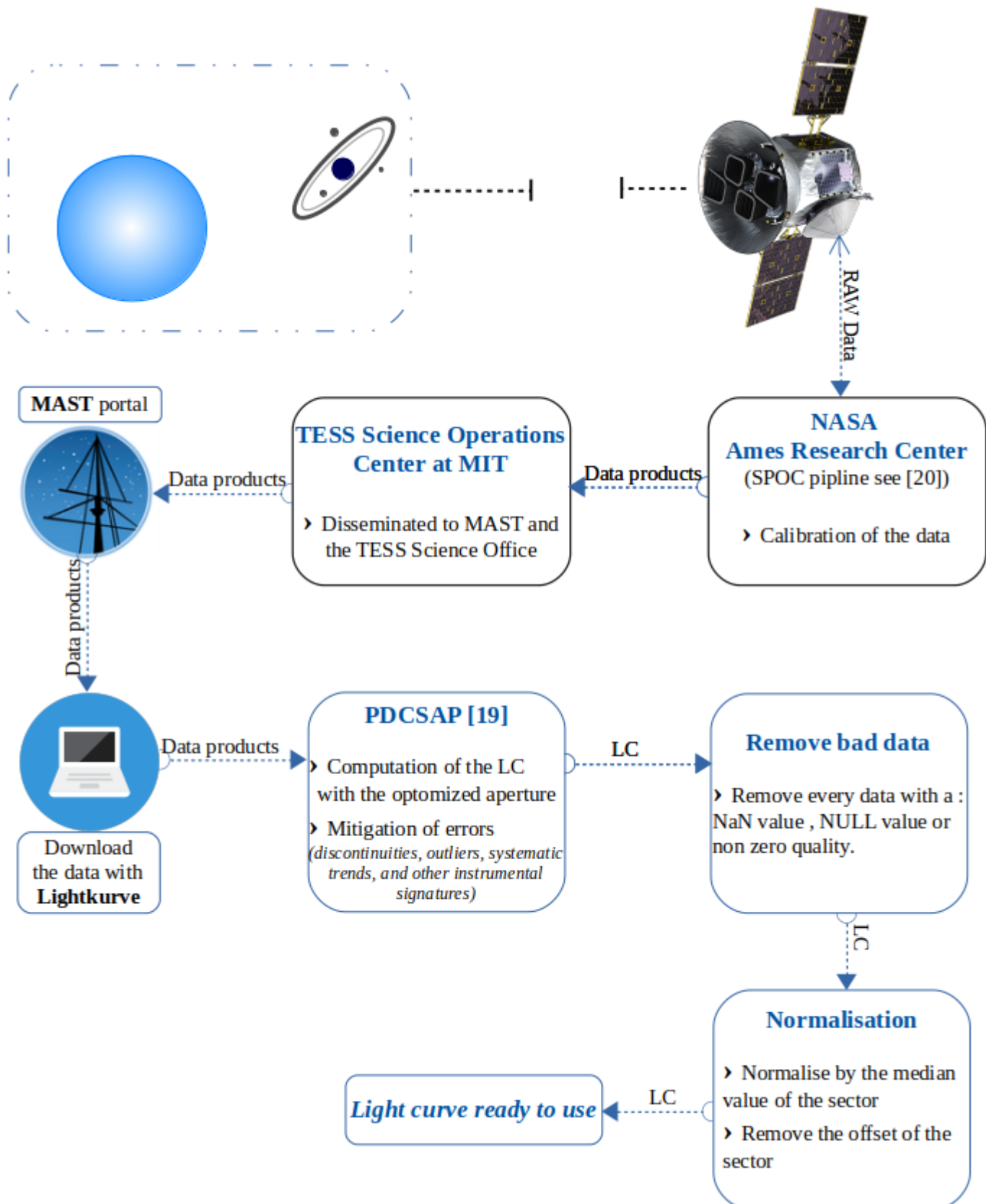


Figure 3.18: Flux of the three reference stars computed with PDCSAP pipeline

#### 3.2.1 The pre-process

After having studied the various ways to extract and process the flux of the star and search for reference stars, we decided to choose the steps described in fig.3.19.

Figure 3.19: The steps to obtain the final light curves



## 4 Comparison between $\beta$ -Pictoris and the reference stars

### 4.1 Transit identification

The light curves of the targets studied by **TESS** are automatically studied to try to detect planet transit. The summary of this study is provided in the Data Release Note [16]. Every potential planetary transit is analysed and fitted. All the information about the planetary fit and the transit detected are stored in the Data Validation files that are available at the url : [https://archive.stsci.edu/tess/bulk\\_downloads/bulk\\_downloads\\_fpi-tp-lc-dv.html](https://archive.stsci.edu/tess/bulk_downloads/bulk_downloads_fpi-tp-lc-dv.html).

The pipeline only detects two transits in the sector 5 ( $t_1 \sim 1442.4$  BTJD and  $t_2 \sim 1459.1$  BTJD). The pipeline failed to identify the transit that appears in sector 6 firstly. However this transit was highlighted a Data Validation paper that cover sectors 1 through 6.

### 4.2 Identification of the momentum dumps

Even if the momentum dumps are supposed to be well identified by the data quality flag, we have to mark (see tab.4.8) them clearly to do a proper comparison between the referenced stars and Bpic. As we can see on the curves obtained with the SAP pipeline (see fig.3.15) the effect of the momentum dumps could last about 1.5 days while the effect on the pointing is supposed to last 15 minutes (cf § 8.2.4 [14]). Even if, the PDC pipeline partially correct the effect of the momentum dumps and the effect of the momentum dump that appears during the manoeuvre are marked with a non-zero quality flag, It is important to check the proximity between any potential transit and momentum dumps.

Table 4.8: Identification of the momentum dumps (md) in sectors 5 to 7

Num Sector	Num md	star md	mid md	end md
5	1	1441.0248767809514	1441.029043504423	1441.0332102278446
5	2	1444.0263027643678	1444.0297750249913	1444.0332472855764
5	3	1447.0263316856356	1447.0298039359952	1447.0332761863551
5	4	1450.0263498144222	1450.0298220486977	1450.0332942828948
5	5	1451.5527460735864	1451.5541349742814	1451.5555238750146
5	6	1454.588883365642	1454.5923556140026	1454.5958278624032
5	7	1457.588902046664	1457.5923742858865	1457.5958465250312
5	8	1460.5889123700233	1460.5923845987688	1460.5958568275535
5	9	1463.5889116402388	1463.5916894096529	1463.5889116402388
6	1	1468.3791946488022	1468.3833613189397	1468.3875279890608
6	2	1471.5055816795855	1471.5090538946715	1471.5125261097578
6	3	1474.6305703159414	1474.634042519406	1474.6375147228316
6	4	1481.2763659723273	1481.2798381768205	1481.283310381313
6	5	1484.401345668717	1484.4048178634691	1484.4082900582598
6	6	1487.5263162805218	1487.5290940276082	1487.5263162805218
7	1	1491.6276305452097	1491.6297138598047	1491.6276305452097
7	2	1494.7970430711478	1494.800515253506	1494.7970430711478
7	3	1497.9220029291807	1497.9254751020517	1497.9220029291807
7	4	1501.046953894354	1501.0504260563396	1501.046953894354
7	5	1504.7024417335542	1504.7038306026552	1504.7024417335542
7	6	1507.8593381011965	1507.862810265918	1507.8593381011965
7	7	1510.9842824116668	1510.987754567579	1510.9842824116668
7	8	1514.1092184580216	1514.1119961746417	1514.1092184580216

### 4.3 Smoothed light curves

We have decided to use the brightest stars (see tab.3.6) to compare them with Bpic. Also we smoothed the curves in order to see common trends which were not linked to the pulsations of the star but more like transit or momentum dumps. So that we decided to smooth with a moving average on 240 points which is equivalent to 480 minutes (0,33 days). So that, this is enough to suppress the  $\delta$ -Scuti pulsations ( $T_{\delta S} \in [0.02, 0.3]$  day cf [2]) and we do not suppress the transit events as they last about 1 day.

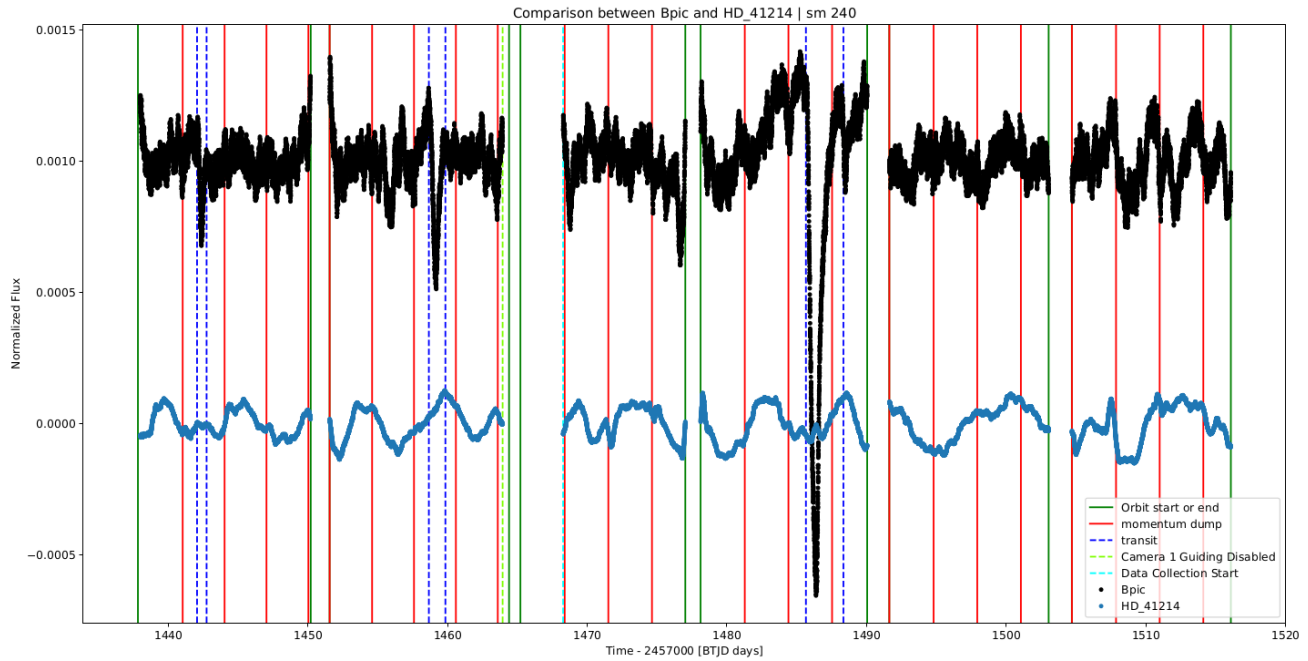


Figure 4.20: Comparison between smoothed curves of Bpic and HD 41214

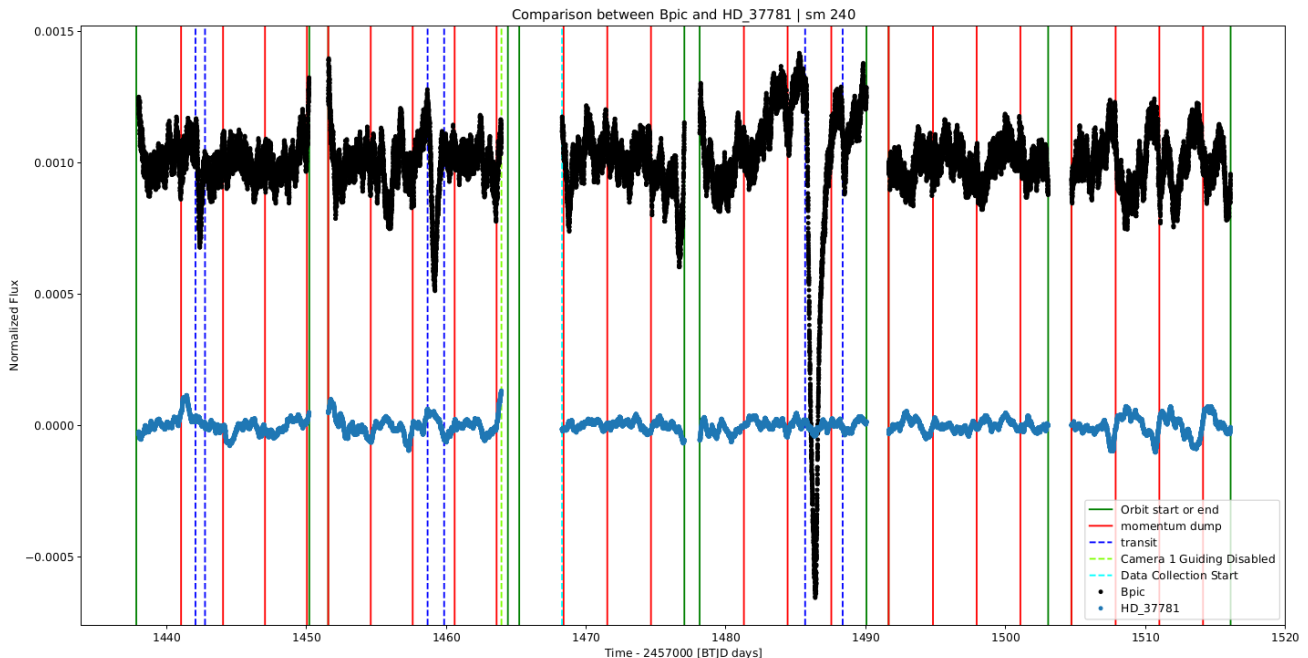


Figure 4.21: Comparison between smoothed curves of Bpic and HD 37781

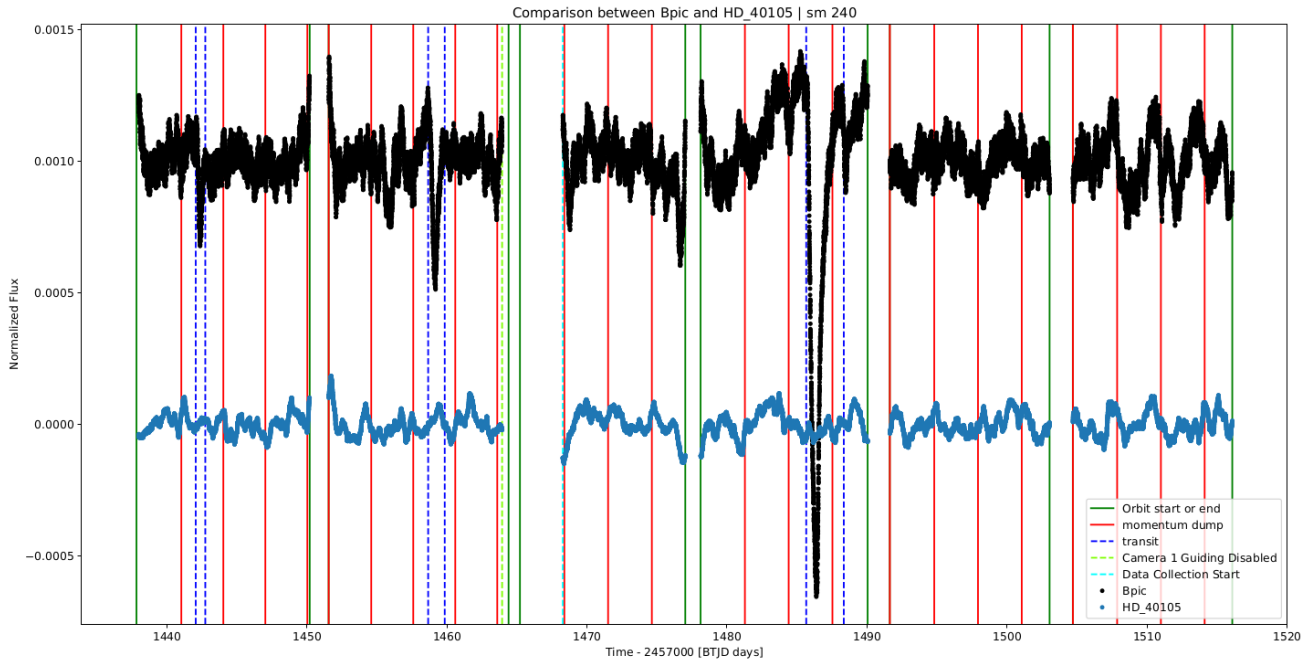


Figure 4.22: Comparison between smoothed curves of Bpic and HD 40105

When we compare the smooth flux of Bpic with the 3 reference stars ( see fig.4.21, fig.4.22 and fig.4.20). We do observe that the variation of the flux of these stars is not the same although we do observe some similarities. So that the variations observed might not only result from instrumental noise and the instrumental noise may affect the flux of the stars in the same way. Still we do observe that the increase of Bpic flux (from 1480 to 1485 BTJD) before the transit in sector 6 does not appear. Only the flux of HD 40105 seems to show a similar behaviour. Also the flux off the three reference stars does not show any dimming events similar to the three potential transits that we do observe in Bpic flux.

In Zieba et al. 2019 [15] they used HD 38991 (variable star) and CD-51 1629 (see tab.4.9). The flux of those two stars does not show any dimming events similar to the transit observe in Bpic flux as mention the paper.

	HD 38991	CD-51 1629
TESS identifier	TIC 270574544	TIC 270626557
V mag	8.50	10.099
RA	05 46 46.5297456946 8	05 49 00.3069538399
DEC	-50 51 17.020365952	-50 59 51.098911241
Sp type	A4/5V	F5
Distance to Bpic (arcseconds)	810	1000

Table 4.9: Reference stars used in Zieba et al. 2019[15]

## 5 Extraction of the $\delta$ -Scuti pulsations

### 5.1 Dpass

**Dpass** is a genetic algorithm that allows to fit curves, developed by a collaborator Pascal Rubini. Its purpose is to provide an alternative approach to the iterative fitting algorithms that are mostly used for sinusoids fit problems, especially with the software **Period04**.

#### 5.1.1 Genetic algorithms

Genetic algorithms are evolutionary type algorithms specialized in optimization. The functioning of these algorithms mimics the processes involved in the genetic evolution of life species.

**Overall operation of a genetic algorithm :** At first, we create an initial population of "individuals", where each individual is a candidate solution of the problem (here a set of sinusoid functions - the parameters of each sine, frequency, amplitude and phase being its "genes"). Each individual is rated using either a loss or a merit function, here a fit error metrics. The algorithm applies an evolutionary process to the population, to make it produce variability by crossovers and mutation and select the progressively better and better solutions.

- Crossover : Allows to spread genes in the population.
- Mutation : Allows to explore new gene possibilities to find more suitable genes.
- Selection : Keep the individuals which minimize the cost function (the fit error eq.5.2).
- islet : This technique consists in creating islets of populations to favour the exploration of the research space by reducing the homogenisation trend.

The various processes which are involved in genetic algorithms are classified in two types : exploration, homogenisation ( see tab.5.10). It is important to balance well these two processes so that the algorithm will converge quickly in order to obtain a result within a reasonable time while finding the closest fit to the data while avoiding convergences toward local minima.

Exploration	Homogenisation
Mutation	Crossover
Creation of islets	Selection
	Exchange of individuals between islets

Table 5.10: Type of processes involved in genetic algorithms

#### 5.1.2 Operation of Dpass

We consider a  $S$  signal. We assume that the signal is composed of a finite number of sine wave ( $N$ ) belonging to the space of the sinusoids  $\mathcal{E}_{\sin}$ .

Each sinusoid  $s_i$  is completely defined by three parameters: its frequency  $\omega_i$ , its amplitude  $A_i$  its phase originally  $\varphi_i$ . The goal of this genetic algorithm is to solve the optimization problem of eq.5.1 :

$$\underset{s_i \in \mathcal{E}_{\sin}}{\operatorname{argmin}} \text{rms} \left( S - \sum_{i=0}^N s_i(A_i, \omega_i, \varphi_i) \right) \quad (5.1)$$

$$\left\| S - \sum_{i=0}^N s_i(A_i, \omega_i, \varphi_i) \right\| \quad (5.2)$$

The first step consists in choosing in which subdomain of frequency the algorithm will search for sine components. The choice of the domain is done thanks to physical hypothesis about the nature of the signal (ex : typical frequency range for  $\delta$ -Scuti star pulsations).

Then, we set various parameters of the fit. These hyper-parameters, allows to balance the exploration of the solutions and the converge towards a good local optimum if not the global one. Once the parameters are set, we start the algorithm which will follow the step define in fig.5.23.

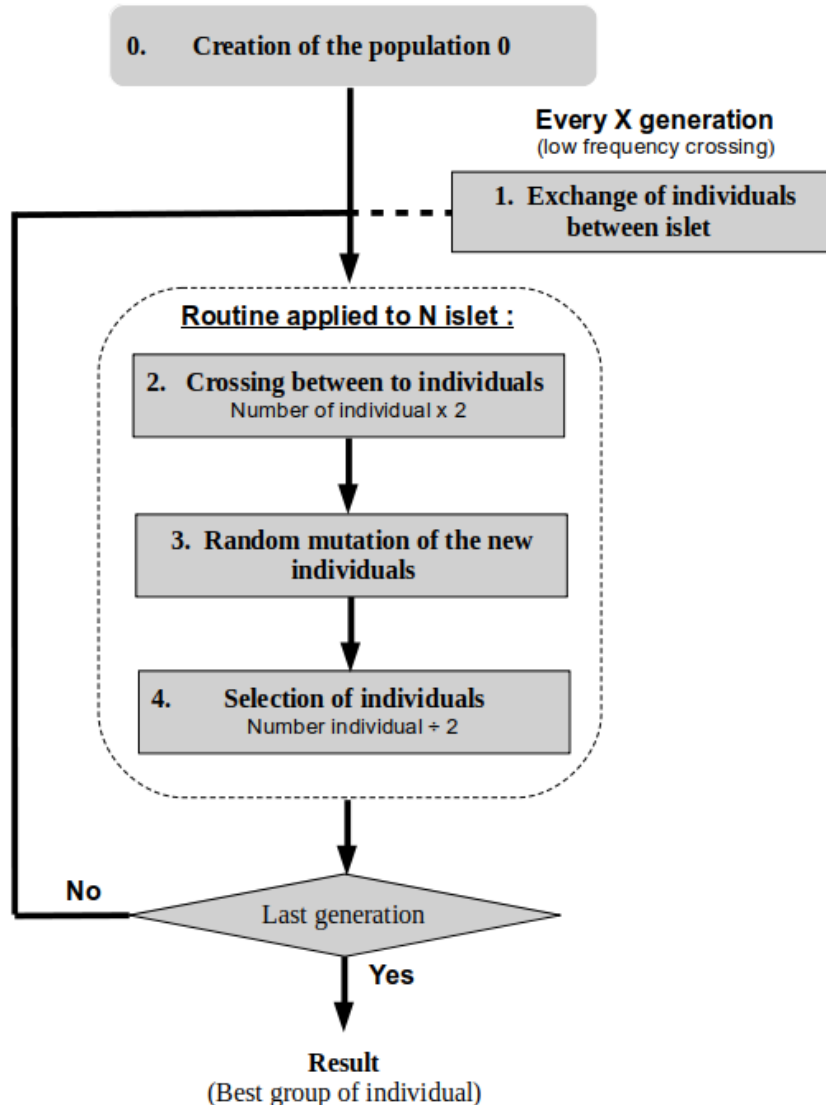


Figure 5.23: Diagram of the operation of dpass

When we do the crossover, we select iteratively two random parents to produce a new child solution and apply random mutations to its genes, until we get a population twice its original size.

Then we proceed to the random mutation step on the new individual of the populations of each islet. Every new individual is potentially mutated with an amplitude also random and configurable (which is adjusted depending on the spreading of the distribution of values of this gene in the population of the islet).

During some of the iteration we proceed to a genetic mixing between the population of each islet (crossing between individuals of different islet). This mixing is done at a low frequency in order to avoid homogenising the populations too quickly.

$$score_{s_i} = \sqrt{\frac{1}{N_{data}} \sum_{j=1}^{N_{data}} S(j) - s_i(t_j)} \quad (5.3)$$

During the selection of the individuals, we calculate the root mean square (rms) of the residual from the subtraction of the individual to the signal (eq.5.3). The value of his rms is used to give a score to each individual of the populations. Then we rank the score of every individual of the population and drop the worst half to restore the original population size.

## 5.2 Iterative algorithms

### 5.2.1 Period04

Unlike **Dpass** the iterative algorithms will try to identify the frequencies one by one, although they can also propose as **Period04** to optimize at the same time all parameters of the frequencies found. The global operation of **Period04** follow the steps show in 5.24.

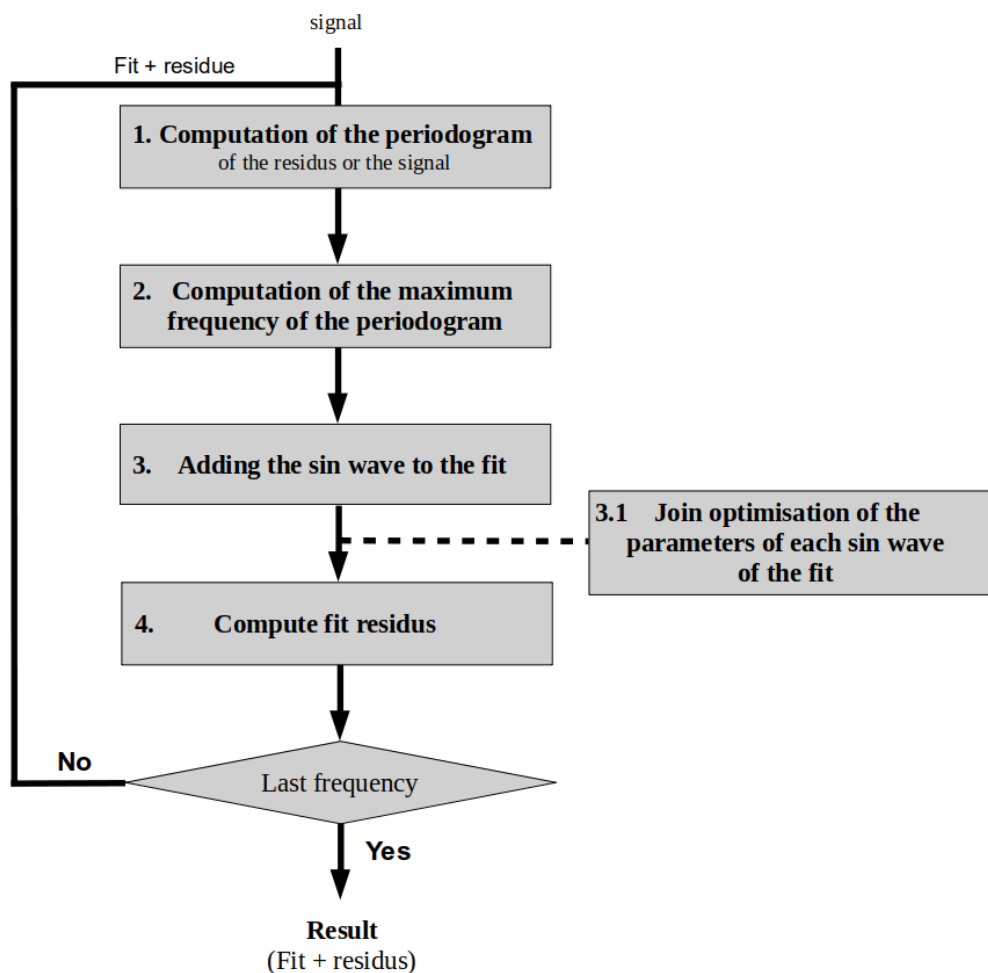


Figure 5.24: Diagram of the operation of period04

### 5.2.2 Fit\_tess

**Fit\_tess** is an iterative algorithm for pulsation extraction developed under **IDL** language by Nadège Meunier. This algorithm was created in order to have our own iterative algorithm to compare the result with dpass.

## 6 Analysis of the pulsation of $\beta$ -Pictoris

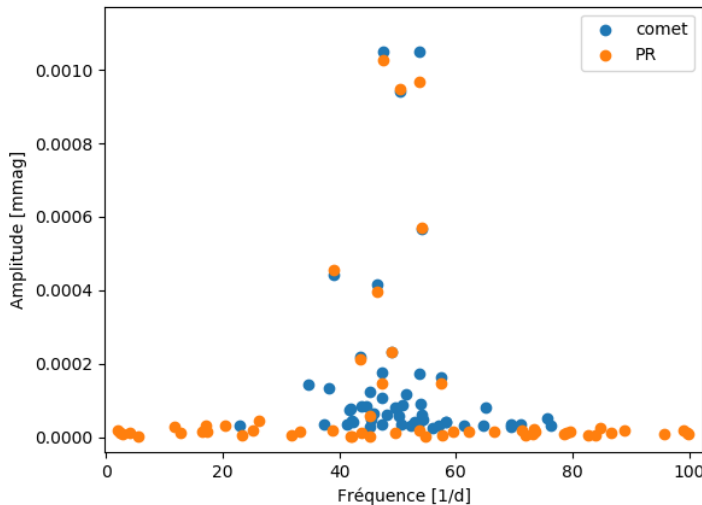
### 6.1 Study of pre-processing of the data

In order to obtain the  $\delta$ -Scuti pulsations of Bpic we used the genetic fit algorithm Dpass (see S.5) . Firstly, we have created various types of times series in order to study the effects of some of the pre-processing on the parameters of the fit produces by Dpass. For instance, we had decided to normalise the curves sector by sector or sub-domain by sub-domain (these sub-domain results of the interruptions that occur during data acquisition (see annexe E).

If the fits dedicated to the study of the domain do calculate the median in order to normalise the data have been done. The result have not been studied as the publication of an article about the data changed the direction of our study.

### 6.2 Comparative study with Dpass

As the research team who wrote the paper Zieba et al. 2019 provide the data they used for the frequency analysis. We could use them with our genetic fit algorithm to see which frequencies would be found be Dpass.



Comet : Frequencies obtained in S. Zieba et al. 2019 [15]

PR : Frequencies obtained by Pascal Rubini with Dpass

Figure 6.25: Comparison of frequencies obtained in Zieba et al. 2019 and with Dpass

We observed on the figure fig.6.25, that the frequencies obtained in the paper Zieba et al. 2019[15] and the one obtained with Dpass share the 10 main frequencies. We note these two methods do not find the same value of the amplitude of the 10 main frequencies. Also we observed that the frequencies found in the paper are in the interval  $20$  to  $80$   $d^{-1}$  while the one find with Dpass are in the interval  $0.1$  to  $100$   $d^{-1}$ . So restrain the domain of frequency research to get the same as the paper.

### 6.2.1 Improvement of Dpass

First, Mr.Rubini and I tried to fit the curves using the same number of sinusoids found in the paper (Zieba et al. 2019 [15])

It turned out that Dpass had real difficulties managing many sinusoids with a strong dynamic amplitude. To overcome this problem we decided to modify Dpass to make it work semi-iteratively. An hyper-parameter constrains the maximum number of sines that can be simultaneously generated (a pass). Multiples passes are performed, each working on the residuals of the previous one. The actual number of components is dynamically determined using periodograms and counting the number of peaks higher than a given fraction of the highest one.

### 6.2.2 Comparison of fit algorithms with a synthetic series

In order to test which of the three fit algorithm would be the more efficient to study the data. M.Rubini tested the efficiency of the three algorithms on a synthetic series created from frequencies found during the previous studies of the pulsation of Bpic. To evaluate the performances of the algorithms he used two indicators (cf eq.6.1, eq.6.2).

With  $X \in \{A, f\}$ ,  $X \in \mathbb{R}^N$  where  $A$  contain the amplitude of the sinusoids and  $f$  the frequencies.

$$mean_{dX} = \frac{1}{N} \sum_{j=1}^N \left| \frac{X_{ref}(j) - X_{fit}(j)}{X_{ref}(j)} \right| \quad (6.1)$$

$$dist_{X,Y} = \frac{1}{N} \sqrt{\sum_{i=1}^N mean_{dX}^2(i) - mean_{dY}^2(i)} \quad (6.2)$$

Algorithms	Frequencies found	$mean_{df}$	$mean_{dA}$	$dist_{Af}$
Dpass (f= 20)	98/100	0.00016360407144793722	0.0951664366735103	0.09518070987275006
Dpass(f = 1)	99/100	5.886272010140221e-05	0.03104548181048226	0.03104722221009046
Tess_fit	99/100	6.149159286787071e-05	0.03215140255929783	0.032153057185018596
Period04	94/100	3.3274372819216973e-06	1.000011940267606	1.0000119403087513

Table 6.11: Result of the comparative test between Dpass et Tess\_fit

We compared the performances of Dpass, Period04 and Tess\_fit by using them on the series synthetic, by setting Dpass for it seeks 20 sinusoids by iteration and then one sinusoids by iteration (see tab.6.11).

We observed that Dpass is more efficient when it seeks for few sinusoids per iteration. Also we see that Dpass is more efficient than Tess\_fit and Period04 when we set it such as it seeks one sinusoids per iteration. Its appears that Dpass is more efficient to find the amplitudes while Period04 is more efficient to find the frequencies.

### 6.3 Creation of the data sets used for the fits

In a first attempt, we created two series with the sectors 5 to 7 of Bpic data. One with the data pre-process as described in fig.3.19 and from which the early beginning of the second orbit of sector 5 has been removed (see fig.6.26). Another one with the data pre-process as described in fig.3.19 and without the data in the vicinity of the three potential transits detected (see fig.6.27). The aim of those two series is to see the impact of the transit on the detection of the pulsations and also to be able to compare with the pulsations founded in Zieba et al. 2019 [15].

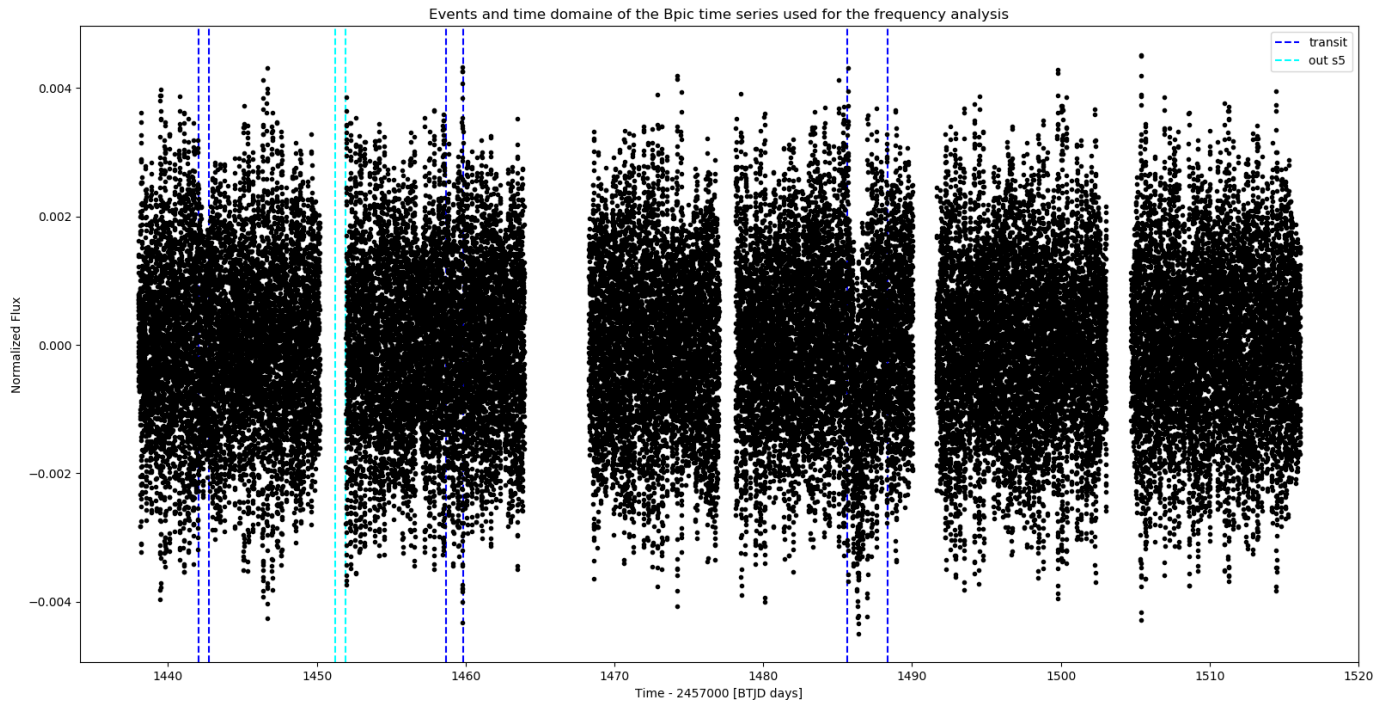


Figure 6.26: Bpic times series of sectors 5 to 7 without the beginning of sector 5

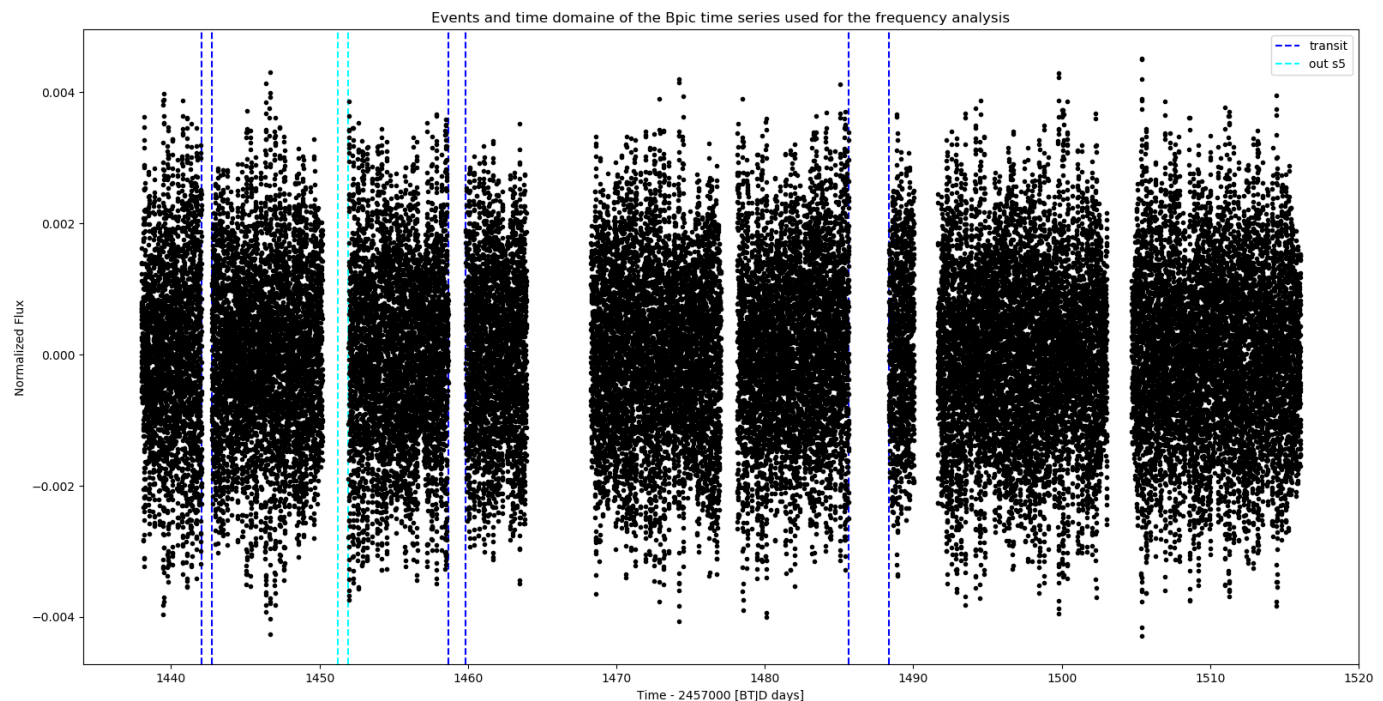


Figure 6.27: Bpic times series of sectors 5 to 7 without the transits events

Then, in order to obtain more accurately the value of the pulsation we studied the smoothed curve of Bpic (see fig.6.29) to see where the data seemed to be unnaturally far from the mean value. We did observed that when an orbit starts or ends the data tend to be deviated from the global trend, especially during sectors 5 and 6. So we decided to remove 74 minute after the begin and before the end of most of the orbit during sectors 5 and 6 (see fig.6.28).

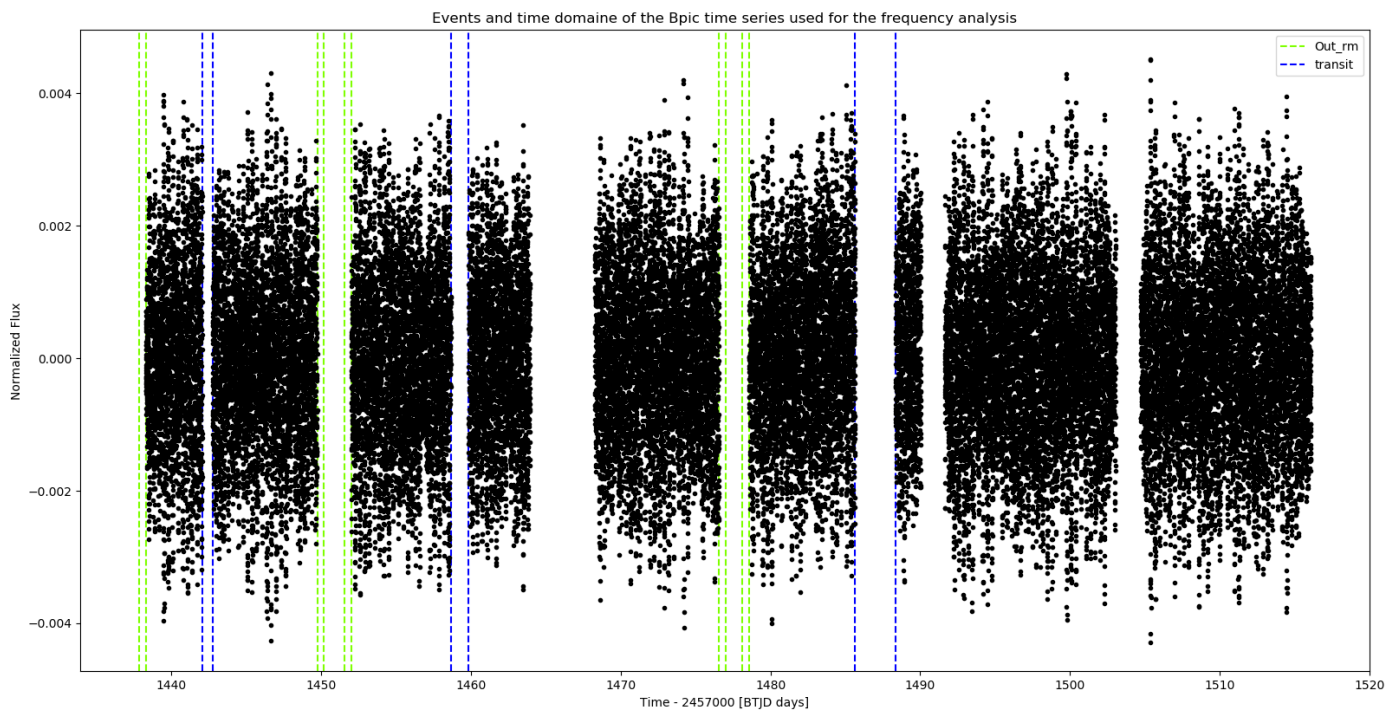


Figure 6.28: Bpic times series of sectors 5 to 7 without the transits events and some of end/start time of the orbits

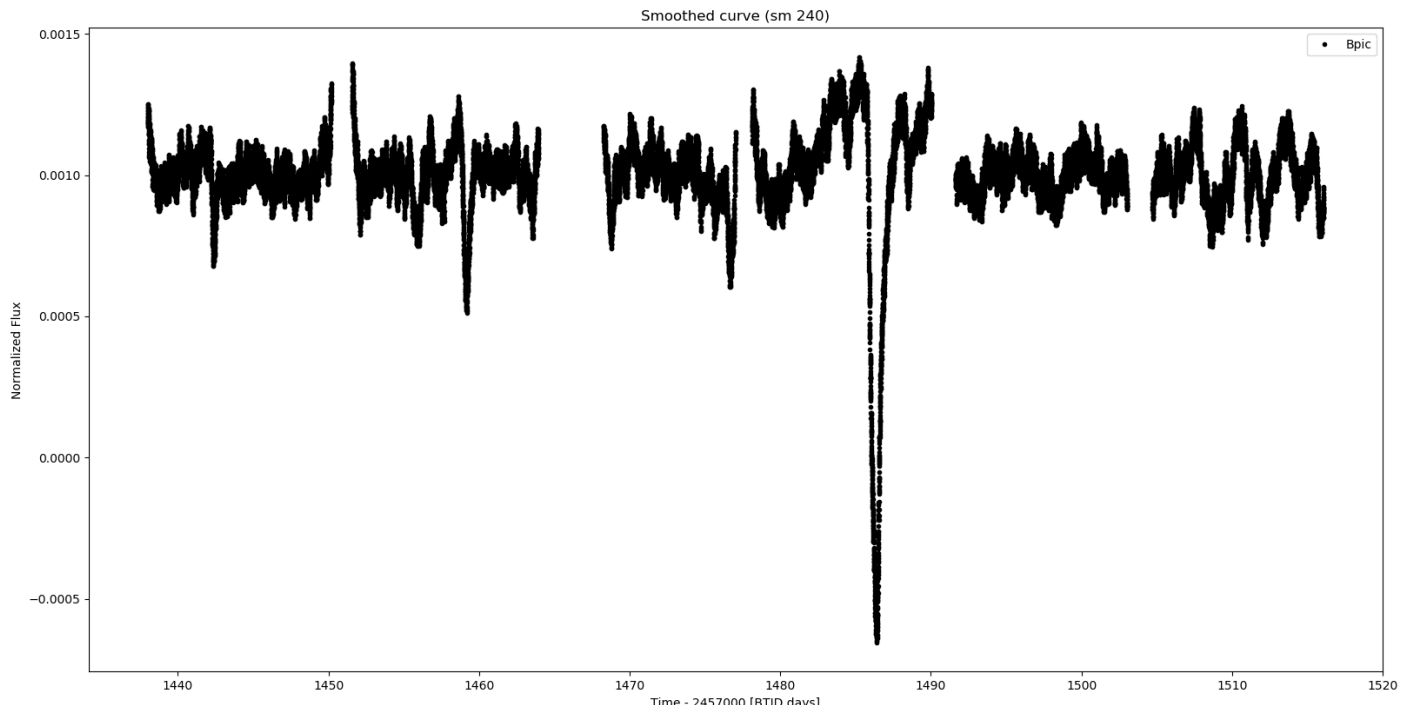


Figure 6.29: Smoothed light curve of Bpic (sectors 5 to 7 | sm = 240)

## 7 Conclusion

In this work we focused on the study of the TESS photometric measurement of  $\beta$ -Pictoris from 19 October 2018 to 1 February 2019 (sectors 4 to 7). We did not study the sector 4 as it was too degraded by spacecraft issues. The publications of Zieba et al. 2019 to find some important document quickly that helped us to get a better overview of the use of the data provide by TESS. Also their result influences us on our choice to modify Dpass in order to make it more efficient to study the data.

In order to analyse the variations of the flux of  $\beta$ -Pictoris we identified three reference stars that were the brightest non-variable stars near to  $\beta$ -Pictoris. After comparing the smooth flux of  $\beta$ -Pictoris with the reference stars that we confirmed that the transit. We note an increase of flux just before the biggest comet transit was not reported by Zieba et al, 2019 [15]. Whether this increase is due to a physical effect connected to the transit of the comet is still to be studied.

### 7.1 Future work

#### 7.1.1 Clustering study of the fits

Now that I have done some fit of the series defines in § 6.3 and the sub series from these series, I will do a clustering study of the result as it has been done in § 6.2. In order to see how the definition of the series study affect the result of the fit. Also, I will try to identify if some the  $\delta$ -Scuti pulsation parameters tend to vary over time.

#### 7.1.2 Analysis of ASTEP data

Then I will do the analysis of the  $\delta$ -Scuti pulsations of Bpic with the data provided by ASTEP. So that I could compare the result with the one found with TESS Data. I will also study the potential variation of  $\delta$ -Scuti pulsation parameters over time as these data covers a large time window.

When we would have properly identified the  $\delta$ -Scuti pulsations of Bpic we will compare the residual flux of Bpic and the flux of reference stars from ASTEP data to see if we do detect the signature of the Hill Sphere transit.

## References

- [1] D. MÉKARNIA, E. CHAPELLIER, T. GUILLOT, L. ABE, A. AGABI, Y. DE PRA, F.-X. SCHMIDER, K. ZWINTZ, K. B. STEVENSON, J. J. WANG, A.-M. LAGRANGE, L. BIGOT, N. CROUZET, Y. FANTEÏ-CAUJOLLE, J.-M. CHRISTILLE, AND P. KALAS 2017 "THE  $\delta$  SCUTI PULSATIONS OF  $\beta$ -PICTORIS OBSERVED BY ASTEP FROM ANTARCTICA".  
<https://www.aanda.org/articles/aa/pdf/2017/12/aa32121-17.pdf>
- [2] STARS QIAN S.-B, LI L.-J., HE J.-J., ZHANG J., ZHU L.-Y. AND HAN Z.-T , 27 DÉCEMBRE 2017 "LAMOST VIEWS  $\delta$  SCUTI PULSATING" .  
<https://arxiv.org/pdf/1707.04006.pdf>
- [3] A.-M. LAGRANGE, D. GRATADOUR, G. CHAUVIN, T. FUSCO, D. EHRENREICH, D. MOUILLET, G. ROUSSET, D. ROUAN, F. ALLARD, É. GENDRON, J. CHARTON, L. MUGNIER, P. RABOU, J. MONTRI, AND F. LACOMBE 2008 "A PROBABLE GIANT PLANET IMAGED IN THE  $\beta$  PICTORIS DISK VLT/NACO DEEP L'-BAND IMAGING" 18 NOVEMBRE .  
<https://www.aanda.org/articles/aa/pdf/2009/02/aa11325-08.pdf>
- [4] FERLET, R., VIDAL-MADJAR, A., & HOBBS, L. M. 1987 "THE BETA PICTORIS CIRCUMSTELLAR DISK. V. TIME VARIATIONS OF THE CA II-K LINE".  
<http://articles.adsabs.harvard.edu/pdf/1987A%26A...185..267F>
- [5] LECAVELIER DES ETANGS, A.; VIDAL-MADJAR, A.; FERLET, R. 1996 "DUST DISTRIBUTION IN DISKS SUPPLIED BY SMALL BODIES: IS THE  $\beta$  PICTORIS DISK A GIGANTIC MULTI-COMETARY TAIL? "  
<http://articles.adsabs.harvard.edu/pdf/1996A%26A...307..542L>
- [6] BEUST, HERVÉ; MORBIDELLI, ALESSANDRO 2000 "FALLING EVAPORATING BODIES AS A CLUE TO OUTLINE THE STRUCTURE OF THE  $\beta$  PICTORIS YOUNG PLANETARY SYSTEM"  
<https://ui.adsabs.harvard.edu/#abs/2000Icar..143..170B/abstract>
- [7] WILSON, P. A.; LECAVELIER DES ETANGS, A.; VIDAL-MADJAR, A.; BOURRIER, V.; HÉBRARD, G.; KIEFER, F.; BEUST, H.; FERLET, R.; LAGRANGE, A. -M. 2017 "FIRST DETECTION OF HYDROGEN IN THE  $\beta$  PICTORIS GAS DISK"  
<https://arxiv.org/pdf/1612.00848.pdf>
- [8] MATRÀ, LUCA; WYATT, MARK C.; WILNER, DAVID J.; DENT, WILLIAM R. F.; MARINO, SEBASTIAN; KENNEDY, GRANT M.; MILLI, JULIEN 2019 "KUIPER BELT-LIKE HOT AND COLD POPULATIONS OF PLANETESIMAL INCLINATIONS IN THE  $\beta$  PICTORIS BELT REVEALED BY ALMA"  
<https://arxiv.org/pdf/1902.04081.pdf>
- [9] M. MOL LOUS, E. WEENK, M.A. KENWORTHY, K. ZWINTZ AND R. KUSCHNIG 2018 "A SEARCH FOR TRANSITING PLANETS IN THE  $\beta$  PICTORIS SYSTEM ?"  
<https://arxiv.org/pdf/1805.05240.pdf>
- [10] WANG, J. J., GRAHAM, J. R., PUEYO, L., ET AL. 2016 "THE ORBIT AND TRANSIT PROSPECTS FOR  $\beta$  PICTORIS B CONSTRAINED WITH ONEMILLIARCSECOND ASTROMETRY"  
<https://arxiv.org/pdf/1607.05272.pdf>
- [11] VAN LEEUWEN, F., ED. 2007, ASTROPHYSICS AND SPACE SCIENCE LIBRARY, VOL. 350, "HIPPARCOS, THE NEW REDUCTION OF THE RAW DATA"
- [12] CHILCOTE, J., PUEYO, L., DE ROSA, R. J., ET AL. 2017 "1 TO 2.4 MICRON NEAR-IR SPECTRUM OF THE GIANT PLANET  $\beta$  PICTORIS B OBTAINED WITH THE GEMINI PLANET IMAGER"  
<https://arxiv.org/pdf/1703.00011.pdf>

- [13] W.R.F.DENT, M.C.WYATT, A.ROBERGE, J.-C.AUGEREAU, S.CASASSUS, S.CORDER, J.S.GREAVES, I.DE GREGORIO-MONSAVOI, A.HALES, A.P.JACKSON, A.MEREDITH HUGHES, A.-M.LAGRANGE, B.MATTHEWS, D.WILNER 2014 "MOLECULAR GAS CLUMPS FROM THE DESTRUCTION OF ICY BODIES IN THE  $\beta$  PICTORIS DEBRIS DISK"  
<https://arxiv.org/pdf/1404.1380.pdf>
- [14] ROLAND VANDERSPEK, JOHN P. DOTY, MICHAEL FAUSNAUGH, JESUS NOEL S. VILLASENOR, JON M. JENKINS, ZACHORY K. BERTA-THOMPSON, CHRISTOPHER J. BURKE, GEORGE R. RICKER, 2018 "TESS INSTRUMENT HANDBOOK"  
[https://archive.stsci.edu/missions/tess/doc/TESS\\_Instrument\\_Handbook\\_v0.1.pdf](https://archive.stsci.edu/missions/tess/doc/TESS_Instrument_Handbook_v0.1.pdf)
- [15] S. ZIEBA, K. ZWINTZ, M. KENWORTHY, AND G. M. KENNEDY, 2019 "A TRANSITING EXO-COMET DETECTED IN BROADBAND LIGHT BY TESS IN THE  $\beta$  PICTORIS SYSTEM"  
<https://arxiv.org/pdf/1903.11071.pdf>
- [16] MICHAEL M. FAUSNAUGH, CHRISTOPHER J. BURKE , DOUGLAS A. CALDWELL, JON M. JENKINS, JEFFREY C. SMITH, JOSEPH D. TWICKEN, ROLAND VANDERSPEK, JOHN P. DOTY, JIE LI, ERIC B. TING, JOEL S. VILLASENOR, 2019, "TESS DATA RELEASE NOTES"  
[https://archive.stsci.edu/tess/tess\\_drn.html](https://archive.stsci.edu/tess/tess_drn.html)
- [17] BREGER, MICHEL MONTGOMERY, MICHAEL ET AL. 2000 "DELTA SCUTI AND RELATED STARS: REFERENCE HANDBOOK AND PROCEEDINGS OF THE 6TH VIENNA WORKSHOP IN ASTRO-PHYSICS" P.7  
<http://www.aspbooks.org/publications/210/3.pdf>
- [18] SARA R. HEAP, DON J. LINDLER, THIERRY M. LANZ, ROBERT H. CORNETT AND IVAN HUBENY, 2000 "SPACE TELESCOPE IMAGING SPECTROGRAPH CORONAGRAPHIC OBSERVATIONS OF  $\beta$  PICTORIS"  
<https://iopscience.iop.org/article/10.1086/309188/pdf>
- [19] SMITH ET AL. 2012 "KEPLER PRESEARCH DATA CONDITIONING II - A BAYESIAN APPROACH TO SYSTEMATIC ERROR CORRECTION"  
<https://iopscience.iop.org/article/10.1086/667697/pdf>
- [20] PETER TENENBAUM, JON M. JENKINS, 2018 "KEPLER PRESEARCH TESS SCIENCE DATA PRODUCTS DESCRIPTION DOCUMENT"  
<https://archive.stsci.edu/missions/tess/doc/EXP-TESS-ARC-ICD-TM-0014.pdf>
- [21] LAGRANGE ET AL. 2019 "POST-CONJUNCTION DETECTION OF  $\beta$  PICTORIS B WITH VLT/-SPHERE"  
<https://www.aanda.org/articles/aa/pdf/2019/01/aa34302-18.pdf>
- [22] F. CRIFO ET AL; 1997 " $\beta$  PICTORIS REVISITED BY HIPPARCOS"  
<http://articles.adsabs.harvard.edu/pdf/1997A%26A...320L..29C>

# Appendix

## Table of Contents

<b>A Annexe : <math>\delta</math>-Scuti stars</b>	<b>35</b>
<b>B Annexe : Transti methods</b>	<b>36</b>
<b>C Annexe : The Exoplanet Team</b>	<b>37</b>
<b>D Annexe : Observation times of TESS sector 5 to 7</b>	<b>38</b>
<b>E Annexe : Time series of <math>\beta</math>-Pictoris obtained by TESS</b>	<b>39</b>
<b>F Annexe : Paper dealings with Bpic TESS data</b>	<b>40</b>

## A Annexe : $\delta$ -Scuti stars

The pulsating  $\delta$ -Scuti star are in the lower instabilitu strip of the Cepheids<sup>22</sup>. The stellar parameters of most of these star are shown in tab.A.12.

Table A.12: Characteristics parameters of the  $\delta$ -scuti stars

Classe	III à V
Spectral types	A2 à F5
Mass	$3 \text{ à } 1.5 M_{\odot}$
Pulsations amplitude	0.003 à 0.9 mag in V band
Pulsations types	Radial and none radial
Period	0.02 à 0.3 days
Pulsation frequency	$3 \text{ à } 80 \text{ days}^{-1}$

source : Stars Qian S.-B et al. 2017 [2]

The amplitude of the variation of most of the  $\delta$ -Scuti star is quite low; The pulsaiton of the  $\delta$ -Scuti star are manly none radial with the index p[17].

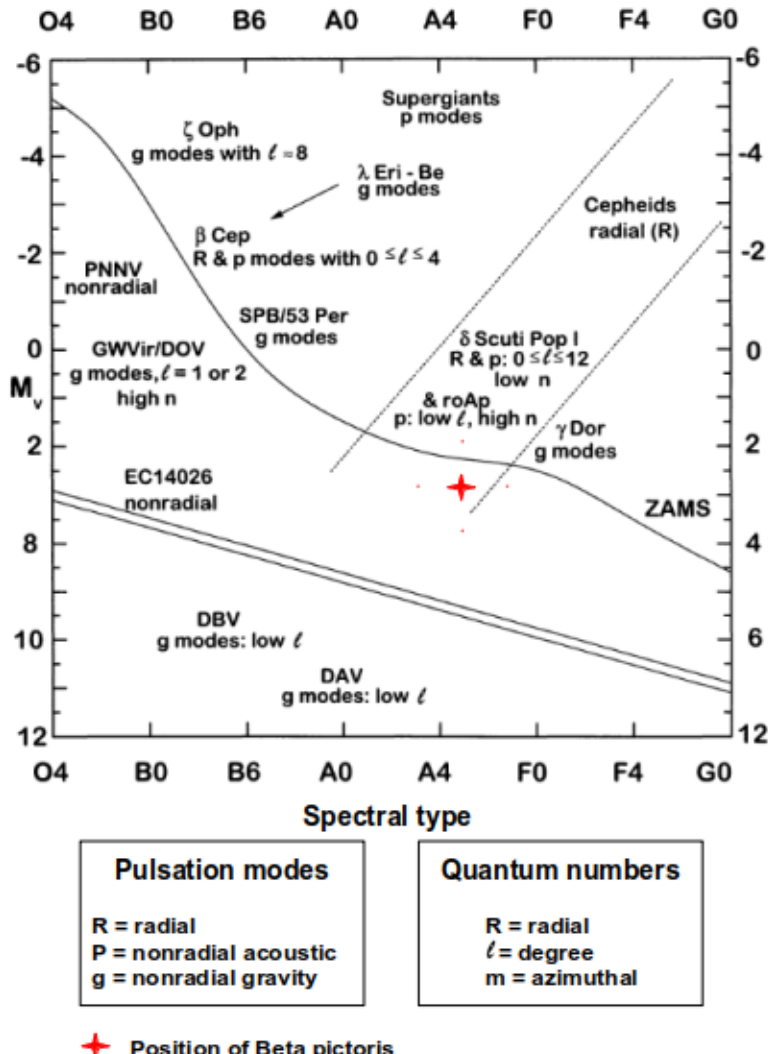


Figure A.30: Position of  $\delta$  Scuti stars in the population I  
source : Michel Montgomery, Michael et al. 2000 [17]

<sup>22</sup>Cepheids are variable stars. <https://fr.wikipedia.org/wiki/C%C3%A9ph%C3%A9e>

## B Annexe : Transti methods

Note : Adapted from the course of Xavier Delfosse (Astronomer at IPAG)

The transits method is a direct type exoplanet detection method. This detection method is mainly represented by scientific missions that are CoRot satellites<sup>23</sup> KEPLER<sup>24</sup> and TESS.

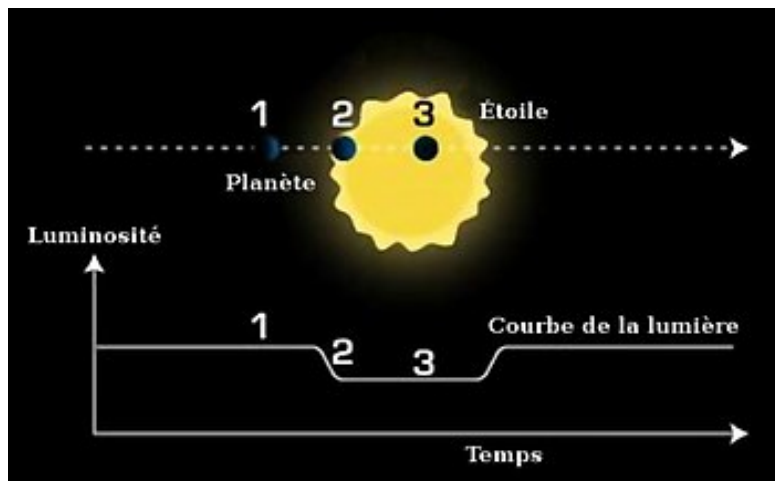


Figure B.31: Illustration of the transit methods

Crédit : Nasa/JPL

This method makes it possible to determine the value of the ratio between the radius of the star and the radius of the planet by means of the calculation of the transit depth eq.B.1. The duration of transit provides information on the orbital period of the planet eq.B.2.

$$\Delta F = \frac{F_{off} - F_{on}}{F_{off}} = \left(\frac{r}{R}\right)^2 \quad (\text{B.1})$$

- $F_{off}$  : Stellar flux outside transit ( $\equiv$  flux 1 on fig.B.31)
- $F_{on}$  : Stellar flux at maximum transit ( $\equiv$  flux 3 on fig.B.31)
- $r$  : Planet radius
- $R$  : Star radius

$$d = 13.0\sqrt{(1-b^2)} \frac{R}{M^{\frac{1}{2}}} a^{\frac{1}{2}} = 1.8\sqrt{(1-b^2)} \frac{R}{M^{\frac{1}{2}}} P^{\frac{1}{3}} \quad (\text{B.2})$$

- $d$  : transit duration (h)
- $R$  : star radius ( $R_\odot$ )
- $M$  : star mass ( $M_\odot$ )
- $a$  : orbital separation ( $UA$ )
- $P$  : orbital period(days)
- $b$  : Impact factor( $R_\odot$ )

<sup>23</sup><https://corot.cnrs.fr/fr>

<sup>24</sup>[https://www.nasa.gov/mission\\_pages/kepler/main/index.html](https://www.nasa.gov/mission_pages/kepler/main/index.html)

## C Annexe : The Exoplanet Team

During my internship I was attached to the team Exoplanètes<sup>25</sup>.

The "Exoplanets" team is strongly invested in the detection and characterization of exoplanetary systems. The team plays a key role in the development and operation of instruments in the context of large international consortia (SPHERE / VLT, SPIRou / CFHT, NIRPS / ESO) or on its own (ERC ExTrA project) on the holding. HARPS / ESO and SOPHIE / OHP and in the longer-term development of an SPHERE upgrade and HARMONI / ELT high contrast arm.

A major objective of these projects is the detection of planets for which characterizations are or will be possible. Characterizations of exoplanet atmospheres (ranging from massive and young Jupiter to terrestrial planets) will be made by exploiting observations in high angular resolution, high spectral resolution, or even cumulating the two. In the near future, the JWST will play a key role for these characterizations, then various ELT instruments will offer unique performances for this theme.

Studies of dynamics and small bodies (debris disks, exozodiacal disks) within extra-solar planet systems provide essential constraints on the architectures and evolution of these systems. They pass notably by heavy modelizations which are essential for interpreting data coming from large radial velocity readings (HARPS, SPIRou), observations in imagery (SPHERE, MATISSE, JWST, ALMA).

Jean-Charles Augereau	UGA astronome
Hervé Beust	UGA astronome
Xavier Bonfils	CNRS chargé de recherche
Mickael Bonnefoy	CNRS chargé de recherche
Alexis Carlotti	UGA astronome adjoint
Xavier Delfosse	UGA astronome
Philippe Delorme	UGA astronome adjoint
Thierry Forveille	UGA astronome
Anne-Marie Lagrange	CNRS directeur de recherche
Fabien Malbet	CNRS directeur de recherche
Nadège Meunier	UGA astronome
David Mouillet	UGA astronome
José-Manuel Almenara	CNRS postdoc
Carlos Gomez	UGA postdoc
Julien Rameau	UGA postdoc
Guillaume Gaisne	UGA doctorant
Antoine Grandjean	UGA doctorant
Lucile Mignon	UGA doctorant
Simon Petrus	UGA doctorant
Laetitia Rodet	UGA doctorant
Christian Romero	UGA doctorant
Elie Sezestre	UGA doctorant

Table C.13: The status of the members of the Exoplanets team  
*source : <https://www.eso.org/public/images/eso0842b/>*

<sup>25</sup><https://ipag.osug.fr/french/recherche/equipes/exoplanetes/>

## D Annexe : Observation times of TESS sector 5 to 7

Table D.14: Sector 4 Observation times

	UTC	TJD <sup>a</sup>	Cadence #
Orbit 15 start	2018-10-19 09:34:28	1410.89974	132081
Guidestar tables replaced	2018-10-21 18:19:59	1413.26468	133783
Instrument anomaly start	2018-10-27 00:52:00	1418.53691	137579
Data collection resumed	2018-10-29 17:03:40	1421.21168	139505
Orbit 15 end	2018-11-01 00:11:40	1423.50890	141159
Orbit 16 start	2018-11-02 01:09:21	1424.54897	141908
Orbit 16 end	2018-11-14 08:21:39	1436.84918	150764

 $TJD^a = TESS\ JD = JD - 2,457,000.0$ 
*source : Michael M. Fausnaugh et al. 2019 [16]*

Table D.15: Sector 5 Observation times

	UTC	TJD <sup>a</sup>	Cadence #
Orbit 17 start	2018-11-15 07:47:48	1437.82566	151467
Orbit 17 end	2018-11-27 16:44:46	1450.19856	160375
Orbit 18 start	2018-11-29 01:09:22	1451.54898	161347
Camera 1 Guiding Disabled	2018-12-11 10:31:39	1463.93945	170269
Orbit 18 end	2018-12-11 21:35:39	1464.40056	170601

 $TJD^a = TESS\ JD = JD - 2,457,000.0$ 
*source : Michael M. Fausnaugh et al. 2019 [16]*

Table D.16: Sector 6 Observation times

	UTC	TJD <sup>a</sup>	Cadence #
Orbit 19	2018-12-12 17:05:01	1465.21262	171185
Data Collection Start	2018-12-15 18:27:38	1468.26998	173387
Orbit 19 end	2018-12-24 12:27:37	1477.01998	179687
Orbit 20 start	2018-12-25 14:41:37	1478.11304	180468
Orbit 20 end	2019-01-06 13:01:37	1490.04359	189064

 $TJD^a = TESS\ JD = JD - 2,457,000.0$ 
*source : Michael M. Fausnaugh et al. 2019 [16]*

Table D.17: Sector 7 Observation times

	UTC	TJD <sup>a</sup>	Cadence #
Orbit 21	2019-01-08 02:59:37	1491.62553	190203
Orbit 21 end	2019-01-19 12:53:3	1503.03803	198420
Orbit 22 start	2019-01-21 04:43:36	1504.69775	199615
Orbit 22 end	2019-02-01 14:01:3	1516.08524	207814

 $TJD^a = TESS\ JD = JD - 2,457,000.0$ 
*source : Michael M. Fausnaugh et al. 2019 [16]*

## E Annexe : Time series of $\beta$ -Pictoris obtained by TESS

When studying the photometric data of TESS we defined study windows (see fig.E.32 and tab.E.18) based on the work done by S. Zieba et al. 2019 [15]. So that we could define 4 subsections in sector 5 as we removed the tow transit and the data are already split in tow part due to the interruption that appears during the change of orbit. We define 3 subsections in sector 6 as we removed the transit and we define 2 subsections in the sector 7.

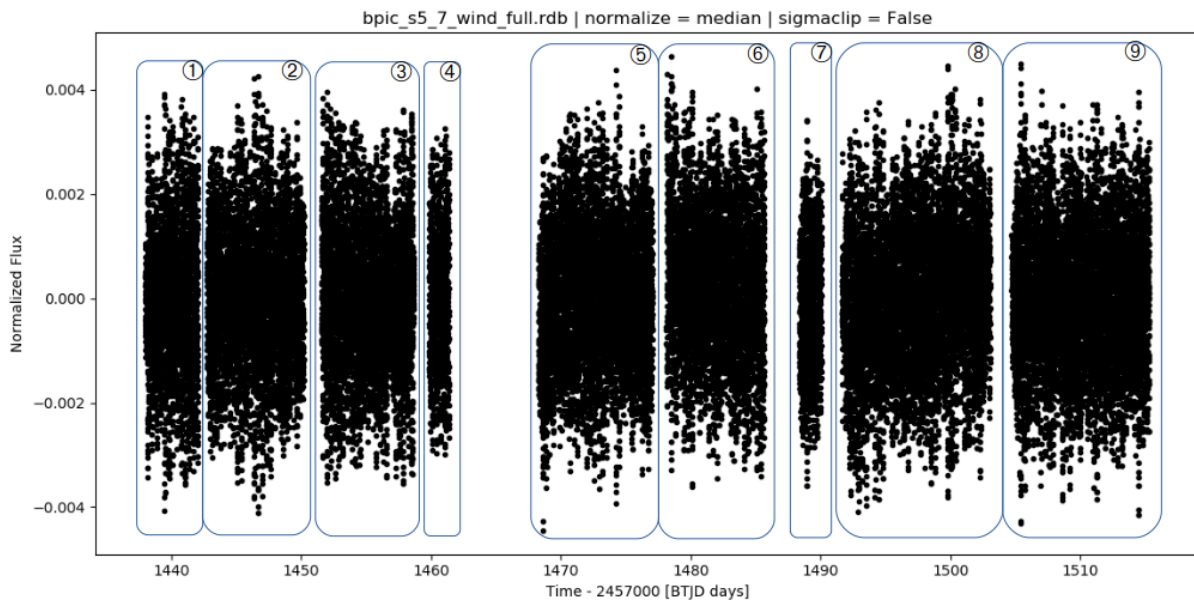


Figure E.32: TESS data, Bpic sectors 5 à 7

Number	Name of the window	Duration (BTJD)
1	bpic_s5_p11	1437,992(88) – 1442,056(83)
2	bpic_s5_p12	1442,742(95) – 1450,186(07)
3	bpic_s5_p21	1451,556(91) – 1458,655(57)
4	bpic_s5_p22	1459,841(68) – 1461,372(24)
5	bpic_s6_p1	1468,273(63) – 1477,022(21)
6	bpic_s6_p21	1478,120(82) – 1485,656(89)
7	bpic_s6_p22	1488,344(36) – 1490,045(72)
8	bpic_s7_p1	1491,633(18) – 1503,038(58)
9	bpic_s7_p2	1504,706(60) – 1515,295(30)

Table E.18: Window definitions

## F Annexe : Paper dealings with Bpic TESS data

An article which deals with TESS data of  $\beta$ -Pictoris data have been submitted (S.Zieba et al. 2019 [15]). The team identified 3 possible transit in the photometric data of Bpic. Two transits with low amplitude has been identified in sector 5 on 1442.5 BTJD and 1459 BTJD. A bigger one, quite visible has been identified in sector 6 on 1486,5 BTJD. The paper is focused on the study of the transit that appears in sector 6 and they assumed that this transit might be due to an exo-comet. The modelization that they carried out pushed them to conclude that the transit to observe in the sector 6 resulted in transit of an exocomet.

The team who published the article has used **Period04** (see § 5.2.1)) to extract the stellar pulsations of Bpic. They found 54 (see tab.F.19) pulsations in the time interval  $22.8145\text{--}76.3167 \text{ day}^{-1}$ . Even if the fit obtained with these pulsation fit quite well the data. We note that in a previous study of the pulsation of Bpic (D. Mekarnia et al. 2017 [1]) another research team have found 31 one pulsations in the time interval  $34.76\text{--}75.68 \text{ day}^{-1}$  of which 10 frequencies have a good level of reliability

Table F.19:  $\delta$ -Scuti frequencies of Bpic found by Zieba et al. 2019

#	Frequency [d <sup>-1</sup> ]	Amplitude [mmag]	Phase	S/N	#	Frequency [d <sup>-1</sup> ]	Amplitude [mmag]	Phase	S/N
1	47.438928(12)	1.048(2)	0.9334(4)	34.3	28	75.6781(2)	0.051(2)	0.416(8)	17.2
2	53.691744(12)	1.048(2)	0.1797(4)	36.4	29	58.3472(3)	0.041(2)	0.117(9)	9.2
3	50.491833(13)	0.940(2)	0.3251(4)	39.6	30	54.2283(2)	0.062(2)	0.411(6)	9.2
4	54.23744(2)	0.568(2)	0.5686(7)	41.7	31	45.4369(3)	0.049(2)	0.910(8)	13.4
5	39.06304(3)	0.442(2)	0.8625(9)	40.4	32	54.4625(3)	0.048(2)	0.198(8)	9.5
6	46.54302(3)	0.414(2)	0.7582(9)	27.3	33	53.5523(3)	0.038(2)	0.143(10)	12.6
7	48.91878(5)	0.230(2)	0.5943(17)	19.1	34	42.1729(3)	0.044(2)	0.557(9)	12.5
8	43.52779(6)	0.217(2)	0.7506(18)	20.6	35	58.2512(3)	0.041(2)	0.309(9)	13.7
9	47.28386(7)	0.175(2)	0.284(2)	22.1	36	42.3960(3)	0.040(2)	0.16(1)	4.7
10	57.45209(8)	0.163(2)	0.203(2)	27.0	37	52.9223(3)	0.040(2)	0.54(1)	9.0
11	34.76041(9)	0.143(2)	0.914(3)	37.4	38	53.68985(7)	0.174(2)	0.607(2)	15.5
12	38.12911(9)	0.133(2)	0.789(3)	33.2	39	57.0484(4)	0.032(2)	0.928(12)	15.4
13	45.26957(10)	0.122(2)	0.705(3)	15.9	40	50.6455(4)	0.033(2)	0.050(12)	6.7
14	51.49625(11)	0.118(2)	0.327(3)	15.5	41	37.4786(4)	0.033(2)	0.636(11)	6.6
15	47.27019(12)	0.108(2)	0.111(4)	15.5	42	69.3752(4)	0.033(2)	0.357(12)	13.7
16	53.85463(14)	0.090(2)	0.419(4)	13.0	43	41.3189(4)	0.033(2)	0.422(12)	18.9
17	49.71250(16)	0.077(2)	0.218(5)	12.9	44	61.4461(4)	0.032(2)	0.434(12)	4.3
18	50.83102(15)	0.087(2)	0.612(4)	15.7	45	22.8145(4)	0.031(2)	0.946(12)	4.3
19	43.82885(15)	0.083(2)	0.068(5)	12.9	46	64.6154(4)	0.030(2)	0.763(13)	4.2
20	65.13492(15)	0.082(2)	0.288(5)	24.1	47	71.0441(4)	0.036(2)	0.016(11)	4.2
21	44.68340(15)	0.083(2)	0.151(5)	16.9	48	52.3034(4)	0.031(2)	0.909(12)	8.8
22	49.55926(16)	0.079(2)	0.297(5)	14.9	49	47.4101(4)	0.035(2)	0.914(11)	10.0
23	42.03524(16)	0.077(2)	0.173(5)	16.7	50	76.3167(4)	0.030(2)	0.898(13)	10.4
24	41.65028(17)	0.073(2)	0.850(5)	18.2	51	45.3553(4)	0.028(2)	0.307(14)	10.1
25	48.1378(2)	0.062(2)	0.744(6)	15.4	52	53.4991(4)	0.031(2)	0.764(12)	8.2
26	45.90034(20)	0.064(2)	0.896(6)	14.3	53	69.5526(5)	0.027(2)	0.687(14)	4.6
27	50.2686(2)	0.056(2)	0.228(7)	15.8	54	56.1099(5)	0.026(2)	0.005(15)	4.0